Energy Conversion and Management 269 (2022) 116183

Contents lists available at ScienceDirect

Energy Conversion and Management

journal homepage: www.elsevier.com/locate/enconman

The dimensional design of a laboratory-scale fluidized bed gasifier using machine learning based on a kinetic method

Furkan Kartal, Uğur Özveren *

Department of Chemical Engineering, Marmara University, Goztepe Campus, 34722 Kadikoy/Istanbul, Turkey

ARTICLE INFO

Keywords:
Kinetic modeling
Gasification
Circulating fluidized bed gasifier
Aspen Plus
ANN

ABSTRACT

Gasification provides various environmental and technological advantages, and the efficiency of the gasification system is affected by several factors, including the kind of fuel and gasification agent used, the gasifier's length and diameter, the operating pressure and temperature, etc. Experimental optimization approaches are more realistic, but they are time demanding; also, a reactor operating at high temperatures and pressures could be dangerous and expensive. Thus, researchers use a variety of modeling techniques, including the process simulators. Additionally, artificial neural network (ANN) as a machine learning approach, which is one of the process modeling methods, is a remarkable approach, and several papers have been published in which it has been utilized in combination with other modeling techniques. On the other hand, a combined process simulator/ANN model that considers gasifier design/operational parameters for the kinetic modeling of gasification process has not been reported.

In this study, after kinetic modeling and validation of seven different circulating fluidized gasifiers using Aspen Plus, parametric studies were performed. Parametric analysis was used to examine the impacts of gasifier diameter, length, gasifier temperature, air/fuel ratio, and fuel type, and a dataset was created for ANN training. The syngas composition and thermal value were predicted using the ANN model. Therefore, a model was developed that takes into consideration both design and operating variables. The investigations revealed that heterogeneous reactions were the most critical factor in defining syngas characteristics. Although design factors have a considerable impact on syngas characteristics, the gasifier temperature is a key factor in the whole process. Furthermore, the ANN model estimates syngas specifications with great accuracy ($R^2 > 0.99$ and MAPE $< 3\%$) based on fuel attributes and gasifier design/operating parameters. Hence, ANN models can be used to analyze the effectiveness of systems including a complex combination of reactions and thermochemical processes.

1. Introduction

Industrial and daily activities rely heavily on energy, yet power generation is still mostly focused on two sources: nuclear energy and fossil fuels. In addition, as a result of the massive industrialization and population growth of the past century, fossil fuel use has increased. However, NO_x, SO_x, CO_2, heavy metals, and $PM_{2.5}$ emissions resulting from the use of fossil fuels remain noteworthy. Thus, due to diminishing fossil fuel reserves, increased environmental awareness, and the dangers of nuclear energy usage, the world is seeking for creative, eco-friendly, stable, and sustainable alternative energy sources. In terms of energy production, renewable resources have lately been seen as providing the opportunity to ultimately substitute nonrenewable sources [1]. In the following years, renewable energy technology research and applications are anticipated to increase. The replacement of nonrenewable energy sources in the global energy distribution is becoming essential [2].

Gasification seems to be an essential process for creating power and other chemical products in a more environmentally friendly and cost-effective approach. Currently, gasification is viewed as a more desirable thermochemical conversion with significantly increased efficiency. It can also be utilized for a multitude of purposes, including the production of heat, electricity, fuels, and chemicals [3]. By heating carbonaceous solids in oxygen-enriched air, carbon dioxide, steam, air, oxygen, or a mixture of these atmospheres, carbonaceous solids are transformed into gaseous fuels. The obtained gas has a better quality standard and is easier and more versatile to use than the raw solid

* Corresponding author.
E-mail address: ugur.ozveren@marmara.edu.tr (U. Özveren).

https://doi.org/10.1016/j.enconman.2022.116183
Received 18 July 2022; Received in revised form 17 August 2022; Accepted 24 August 2022
Available online 1 September 2022

material; for instance, it may be used in gas turbines and gas engines, or as a chemical ingredient to manufacture liquid fuels. Syngas is the term given to the producer gas, the great majority of which consists of H_2, CO, CO_2, N_2, and a few hydrocarbons [4]. Trace amounts of tars, NH_3, and H_2S could also be detected [5].

Moisture evaporation, pyrolysis, oxidation, and reduction are all phases of the gasification process, and they must be carried out under optimal conditions for the most efficient end product. The operating temperature of gasification has a considerable effect on product distributions. Temperature influences the composition and productivity of gas, the calorific value of gas, the formation of char and tar, the cold gas efficiency, and carbon conversion. Further, the equivalence ratio (ER) is a crucial component in defining gasifier properties such as the composition of producer gas. On a dry ash free basis, the ER is calculated by dividing the quantity of oxygen supplied by the amount of oxygen required for complete combustion. The ER must be in the band of 0.2–0.4 for appropriate gasification [6]. The gasification environment has a significant impact on the composition and quality of syngas. The kind of gasifying agent used is decided by the appropriate gas content and energy consumption. Moreover, residence time has a significant impact on both the tar production and syngas composition. Higher residence time considerably improves hydrogen yields and gasification performance. Diverse solid substances have varied chemical compositions, and even portions of the same raw material might have distinct properties and qualities. In fact, biomass/coal heterogeneity is one of the disadvantages of gasification, as it makes it difficult to determine the optimal operating conditions and end product characteristics [7]. In addition to a number of other factors, the height and diameter of the gasifier are crucial criteria that impact the quality of the produced gas [8,9]. Changes in the reactor's diameter or height influence the gasifier's residence duration, temperature distribution, and reactor regime, among several other factors.

Fixed bed gasification was one of the first and most commonly used reactors for the production of syngas [10]. The earliest and most fundamental method of gasification is the fixed bed or moving bed gasifier. It is the most affordable and optimum option for small-scale activities. Researchers and industry experts are interested in the fixed bed gasifier because to its uncomplicated operation and design with no or few moving parts; nevertheless, the produced syngas has a low calorific value and a high tar content [3]. The entrained flow gasifier is designed to accommodate particles between 75 and 100 μm in size. It will first be used to gasify fine coal at extreme temperatures between 1400 and 1800 °C and high pressures between 20 and 70 bar in order to completely degrade tar and provide tar-free syngas [11]. It has a residence time of around 1–5 s. Due to the tiny particle size, high pressure, and temperature, carbon conversion is almost complete. Furthermore, the fluidized bed reactor surpasses the fixed bed gasifier in terms of mixing capacity and heat transfer efficiency due to its fluidization process. The fluidized bed gasifier provides a more consistent temperature response. In a fluidized bed gasifier, high mixing conditions between solid fuel and gasifying agent accelerate feedstock degradation, hence enhancing reaction rate, performance, and conversion. This temperature uniformity may be easily achieved by utilizing bed materials to encourage fluidization of the feedstock [10], so enabling gasification to occur in a nearly isothermal environment. In general, the fluidized bed gasifier operates between 800 and 1000 °C [12]. In circulating fluidized bed gasifiers, the fluidization process is more turbulent and the fluidization velocity is three to five times more than in bubbling fluidized bed gasifiers. As a result of the increased fuel contact with the bed particles and gasification reagent, heat transport and reaction rate are both raised. Since there are too many particles in the freeboard segment, recirculation of solid materials is required. As a consequence, circulating fluidized bed gasifiers have enhanced gasification efficiency and carbon conversion while forming very less tar.

In the development of gasifiers, experimental or computer simulation data is used. Variations in any of the aforementioned factors have a tremendous effect on the end-gas composition and gasifier's performance [13]. Identifying the ideal gasifier design parameters for a specific feedstock may be a time-consuming and expensive task. In this regard, computer simulations have proved valuable for understanding how a gasifier operates and how to improve it prior to the construction of actual prototypes [14]. It may be difficult to quantify the effect of construction, operating, and input factors on reactor performance, but numerical techniques have proved useful in this regard. Four categories of models may be used to determine the gasification process: reaction kinetic modeling, data driven modeling, computational fluid dynamic (CFD) modeling, and thermodynamic modeling [15].

Modeling of thermodynamic equilibrium is often referred to as zero-dimensional modeling [16]. The gasification system is most stable in its equilibrium state. All chemical processes and substances are accounted for in stoichiometric equilibrium models. The non-stoichiometric equilibrium technique primarily focuses on minimizing the Gibbs free energy of the system. Numerous tools such as MATLAB [17], Aspen Plus [18,19], Engineering Equation Solver [20], Aspen HYSYS [21], etc. have been used in thermodynamic modeling, which is extensively practiced and thoroughly reported.

CFD can be used to examine the physicochemical occurrences in a virtual environment under various operating conditions. To accomplish this, CFD models include conservation of mass, molecular momentum, energy flow, hydrodynamics, and a knowledge of the interactions between the many phases and events inside the reactor. The CFD element matrix may be used to develop CFD tool equations including fluxes of the investigated variables entering and exiting the control zone with appropriate boundary conditions. CFD software is used to study all modifications and interconnections in the gasifier, including particle vaporization, carbonization, and gasification processes [22]. The flow dynamics process in a fixed-bed reformer was studied by Pashchenko [23] using both computational and experimental approaches. The purpose of the research was to determine how different particle shapes affect the pressure drop and loss factor in a packed fixed bed containing a porous catalyst. Article implies that there is a good correlation between numerical and experimental findings for all studies, with an average error of <8%. Furthermore, Enget and Jaojaruek [24] simulated a downdraft gasifier operating on cubic woodchips and air. In order to simulate how biomass is positioned when fed into a gasifier from above, woodchips were individually inserted into the gasifier in a disorganized manner. The authors discovered that CFD analysis is helpful in determining the pressure drop in gasifiers using loose biomass feedstock when empirical correlations are not available. Further, bed pressure drop and bubble behavior in bubbling fluidized beds provided by a shroud nozzle distributor were calculated using computational particle–fluid dynamics (CPFD) simulations by Lim et al [25]. Each simulation's pressure drop profile was compared to experimental data obtained under the identical circumstances to ensure accuracy. Without proper implementation of the collision and particle normal stress models in the simulation, the predicted bed pressure drop and bubble flow characteristics did not correlate with the experimental data. Due to a lack of computer power, CFD models for gasification are infrequent [10]. Nonetheless, CFD modeling of different types of gasifiers has been reported in the literature [26–29].

Kinetic models can investigate a deeper variety of parameters than equilibrium models can. Kinetic modeling systems are founded on kinetic principles, which are essential for the design, evaluation, and enhancement of gasifiers because they represent the chemical interactions that occur throughout the process. Models may be used to predict residence duration, gasifier design, flow rates, and gasifier hydraulics, among other characteristics [30]. Agu et al. [31] developed a one-dimensional model that incorporates the hydrodynamic behavior of a fluidized bed. The authors included the momentum equations of fuel particles and fluid into their model. The model's conclusions were validated using experimental data, and the proposed model was capable of projecting total gas production and product gas composition under a

variety of operating conditions. Furthermore, in order to simulate the gasification of rice husk in a bubbling fluidized bed gasifier, Xiong et al. [32] used a kinetic model that included both flow hydrodynamics and chemical kinetics. Their model was based on the two-phase fluidized theory, which postulates that the bed contains two phases that transfer energy and mass. According to their parametric study, bed diameter had a negligible effect on gasifier performance, however raising reactor temperature and bed height improved gasifier performance. Nonetheless, biomass moisture and gasification agent entrance velocity had differing impacts on the performance of the gasifier. Nemtsov and Zabaniotou [33] simulated the gasification of agricultural wastes in a fluidized bed gasifier, taking into consideration the various stages of the process. According to the authors, mathematical modeling may not only be used to account for the fundamental behavior of fluidization and the gasification process, but also as a forecasting tool for fluidized bed gasifier design, modification, and scaling up. In recent study, Hejazi and Grace [34] modeled calcium-looping in a dual fluidized bed reactor's bubbling fluidized bed carbonator for the synthesis of H_2-rich syngas using the FluidBed module of Aspen Plus v10. Comparing the experimental findings of a 20 kW_{th} dual fluidized bed gasifier operating in Ca-looping and delivering tar-free synthesis gas. According to their findings, using tar- and impurity-free syngas for feedstock increases CO_2 capture efficiency and increases syngas H_2 content from 51.4% to 80%.

Due to their strong generalization capacity, artificial neural networks (ANNs) have recently acquired popularity for tackling difficult actual engineering and scientific problems [35]. In contrast to kinetic modeling and CFD, which both need a great deal of computing power, ANN provides an alternative modeling technique that uses less computational power and has a quicker execution time while keeping appropriate accuracy. The ANN-based modeling methodologies may consistently and quickly map complex processes from a collection of samples without requiring understanding of the underlying mechanisms and principles. In other words, ANN-based models may represent complex dynamic systems with multidimensional properties without having a comprehensive understanding of the underlying physical principles. Two ANN model topologies were proposed by Puig-Arnavat et al. [14] for fluidized bed gasifiers. The scientists collected experimental data from several sources and utilized it to train ANNs. For the estimation of gas output and syngas composition, both ANN models use a number of process variables and feedstock content as input variables. Experiments shown that output parameters may be predicted with high accuracy by using a neural network with two hidden neurons in the hidden layer and a backpropagation technique. Excellent correlations ($R^2 > 0.98$) appear between the results achieved by these ANNs and the published experimental data in nearly all cases. In a recent study, Yan et al. [36] used thermodynamic ANN modeling to accurately predict gasification outputs, while the non-dominated sorting genetic algorithm-II was used to evaluate different gasifier design parameters. To train the thermodynamic ANN model, the researchers used 166 experimentally reported data points. The researchers also noted that among the input variables, gasification temperature has the greatest effect, and that the thermodynamic ANN model outperformed the conventional thermodynamic equilibrium and ANN models in terms of accuracy and robustness of prediction. The integration of thermodynamic equilibrium with ANNs and the use of experimental data to train ANNs have been reported. Moreover, simulation data was used for ANN model training in terms of predicting gasification/gasification-driven systems' characteristics [37–40].

Gasification processes are often simulated, however there have been reports of practical investigations examining the impacts of gasifier design for various applications. Using empirical relationships, Dasappa et al. [41] investigated the development of small-scale gasifier designs in India (including many prototypes) with a throat size between 30 and 40 mm. In a similar study, Sutar et al. [42] proposed a design technique for small downdraft gasifiers by modifying existing standards for larger gasifiers. While designing gasifiers with outputs of 2.5 kW_{th} and 4.5 kW_{th} and throat widths of 20 and 30 mm, respectively, the authors used non-linear extrapolation of the design curves. Recently, Khan et al. [43] have proposed and developed a flexible design method for a standard laboratory gasifier test-bed. The objective of the project is the construction of a laboratory-scale throated downdraft gasifier with a sliding throat configuration that will facilitate process optimization and the extrapolation of the findings to larger gasifiers. Moreover, Guangul et al. [44] have designed a downdraft gasifier that enables for the height of the gasifying air and steam inlet to be adjusted. Thus, the designed facility allows for investigating how shifting the air and steam input positions affects the gasification procedure. In conclusion, researchers are interested in modifying gasifiers by constructing models with interchangeable pieces in order to identify the most effective gasifier structure for synthesizing their target materials. Additionally, while building new gasifiers, the researchers modify gasifier capacity based on empirical correlations with preexisting gasifiers. On the other hand, there have been very few reports of research on the adjustable design of lab-scale circulating fluidized bed gasifiers. Though, the advantages of developing a laboratory-scale gasifier include the quick evaluation, identification, and comparison of optimal scaling strategies and process improvements such as feedstock evaluation, tar reduction, syngas cleaning and upgrading, and the evaluation of novel catalysts in various laboratories. This study also aims to fill the gap in the literature by proposing a lab-scale circulating fluidized bed gasifier design using the ANN model trained with kinetic method-based simulation results.

A review of the relevant literature reveals that numerous modeling methodologies have been used for gasification systems. Using CFD for a virtual design is possible, however it is computationally intensive, and thermodynamic equilibrium based models cannot be applied in the gasifier design process. While data-driven models have been proven to be beneficial due to their computational efficiency and capacity to deal with complicated datasets, the majority of existing research has used a single fuel type, a single gasifier size/diameter, and a limited number of operating parameters. The presented models are, thus, only applicable under extremely narrow circumstances. On the other hand, a combined process simulator/ANN model that considers gasifier design/operational parameters for the kinetic modeling of gasification process has not been reported. In this work, parametric analyses were conducted following kinetic modeling and validation of seven distinct circulating fluidized gasifiers using Aspen Plus. Applying parametric analysis, the effects of gasifier diameter, length, gasifier temperature, and air-to-fuel ratio, further, a data set was compiled for ANN training. Using the ANN model, the composition and thermal value of syngas were predicted. Therefore, a model was constructed that takes both design and operation factors into account. Ultimately, a lab-scale fluidized bed gasifier was virtually designed by using the developed ANN model and parametrically investigated to determine optimum operating/design conditions. Therefore, this work employs a dual-modeling strategy to conduct in-depth analysis.

2. Methodology

2.1. Feedstock Characterization

Proximate and ultimate analyses are the most often used methods for characterizing solid fuels. Biomass is more reactive than coal owing to its more reactive char and higher volatile content, but it has a lower calorific value due to its lower carbon and higher oxygen and hydrogen contents [45]. While biomass has a lower energy content, it also contains more moisture and less fixed carbon. Also, biomass has low emissions due to these inherent features, making it an appropriate feedstock material. Table 1 summarizes the results of the ultimate and proximate analyses of the feedstock materials used in this paper.

Through a literature review, the properties of the feedstock materials employed in the kinetics calculations of this study were obtained. A range of solid fuels, including agricultural and forestry wastes and

Table 1
The findings of both the proximate and ultimate analyses of the feedstock materials used in this paper.

Biomass Sample	Moisture	Ash	Fixed Carbon	Volatile Matter	C	H	S	N	O	Ref.
Olive oil waste	8.9[a]	8.5[b]	17.1[b]	74.4[b]	52.7[c]	7.2[c]	0.07[c]	1.6[c]	38.1[c]	[46]
Miscanthus pellets	8.7[a]	2.5[a]	15.0[a]	73.8[a]	43.9[b]	5.9[b]	0.14[b]	0.57[b]	46.8[b]	[47]
Willow	17.0[a]	2.13[b]	16.5[c]	83.5[c]	48.7[c]	5.91[c]	0.045[c]	0.88[c]	44.5[c]	[48]
Sawdust	9.43[a]	1.10[b]	15.63[b]	73.84[b]	52.30[b]	5.17[b]	–	0.40[b]	41.70[b]	[49]
Juliflora chips	12.10[a]	1.86[b]	16.34[b]	81.80[b]	45.55[c]	6.44[c]	0.205[c]	0.583[c]	47.22[c]	[50]
Eucalyptus wood	11.8[a]	2.6[a]	14.6[a]	71.0[a]	45.85[b]	6.13[b]	<100 ppm	0.35[b]	44.80[b]	[51]
Subbituminous coal	10.4[a]	16.0[a]	30.2[a]	43.4[a]	57.2[a]	3.3[a]	0.2[a]	0.7[a]	16.2[a]	[52]

a: as received (ar.) basis, b: dry basis (db.), c: dry-ash free (daf.) basis.

subbituminous coal, were chosen. According to the proximate analysis results provided in the table, the volatile matter content of the biomass samples is high (>70%). However, the proportion of fixed carbon in the coal sample is much higher than in the biomass samples. Fig. 1 depicts the Van Krevelen diagram for the feedstocks studied in this investigation.

The Van Krevelen chart is a technique for recognizing solid fuels and determining their level of carbonization. The O/C and H/C fractions may be used to determine if a fuel belongs to a certain category and its performance. When analyzing the figure, it is apparent that all biomass samples are located inside or close to the biomass zone. Subbituminous coal, on the other hand, is expectedly found in the coal region. In terms of degree of carbonization, subbituminous coal is a superior fuel than other biomass samples. The olive oil waste sample included the highest quantity of hydrogen, whereas the miscanthus pellet sample contained the highest concentration of oxygen. In addition, the sawdust sample had the highest level of carbonization among all the biomass samples.

2.2. Gasification reactions and kinetics

Regardless of technology, gasification reactors include a series of thermal processes, including moisture evaporation and carbonization, oxidation/cracking of pyrolysis products, and char gasification. Total carbon conversion is mostly attributable to the heterogeneous interactions occurring between the char obtained during the pyrolysis process [53]. Due to the high temperatures in the reactor, the rigorous circulation of substances undergoing heterogeneous and homogeneous interactions, and the complexity of the chemical and physical phenomena involved, it would be difficult to experimentally determine the optimal gasification process variables and design. In addition to the reaction scheme described below, kinetic modeling is a potent simplification of the hundreds of chemical processes that occur in a gasifier. The heterogeneous interactions between char and gases are the rate-controlling step in a gasification process, therefore much attention is given to them [54]. The primary reactions in the gasification operation are listed in Table 2.

Due to the absence of data for the different reaction rates and the higher computation needs, a more comprehensive strategy is not feasible. The global approach/mechanism in which reaction rates are calculated empirically from experimental data. Often, the Arrhenius equation is employed to represent these phenomena. The following is the equation for gas-phase interactions [55]:

$$k = AT^{n}\exp\left(-\frac{E_a}{RT}\right)[Fuel]^{a}[Oxidizer]^{b}[3^{rd}]^{c} \quad (1)$$

Table 2
The major reactions occurred during a gasification process [7].

Reaction	Heat of reaction at 25 °C	Reaction Name
$C + CO_2 \leftrightarrow 2CO$	+172 kJ/mol	Boudouard reaction
$C + H_2O \leftrightarrow CO + H_2$	+131 kJ/mol	Water-gas reaction
$C + 2H_2 \leftrightarrow CH_4$	−74.8 kJ/mol	Hydrogasification
$CO + H_2O \leftrightarrow CO_2 + H_2$	−41.2 kJ/mol	Water-gas shift reaction
$2CO + 2H_2 \rightarrow CH_4 + CO_2$	−247 kJ/mol	Methanization reaction
$CO + 3H_2 \leftrightarrow CH_4 + H_2O$	−206 kJ/mol	Methanization reaction
$CO_2 + 4H_2 \rightarrow CH_4 + 2H_2O$	−165 kJ/mol	Methanization reaction
$CH_4 + H_2O \leftrightarrow CO + 3H_2$	+206 kJ/mol	Steam-methane reforming
$CH_4 + 0.5O_2 \rightarrow CO + 2H_2$	−36 kJ/mol	Methane combustion
$C + 0.5O_2 \rightarrow CO$	−111 kJ/mol	Combustion reaction
$C + O_2 \rightarrow CO_2$	−394 kJ/mol	Combustion reaction
$CO + 0.5O_2 \rightarrow CO_2$	−284 kJ/mol	Combustion reaction
$CH_4 + 2O_2 \leftrightarrow CO_2 + H_2O$	−803 kJ/mol	Combustion reaction
$H_2 + 0.5O_2 \rightarrow H_2O$	−242 kJ/mol	Combustion reaction

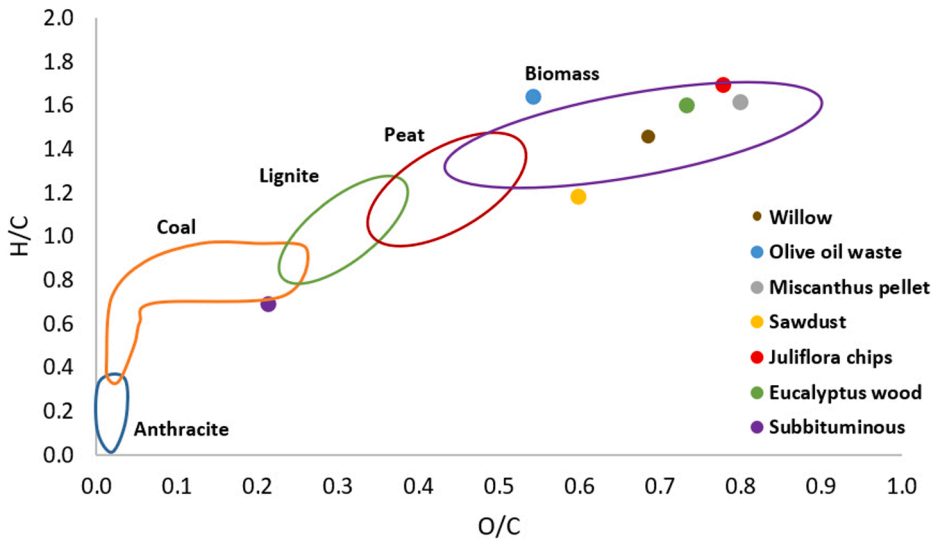

Fig. 1. Characterization of feedstock materials by Van Krevelen diagram.

A – the Arrhenius consant (the unit is determined by the reaction order).

T – absolute temperature (K).

Ea – activation energy.

n – the temperature exponent.

[3rd] – the third species' molar concentration (neither a product nor a reactant).

a, b, and c – concentration exponents.

R – the universal gas constant.

To determine the values of the variables *Ea*, *n*, *A*, *b*, and *a*, one may use experimental data or complex techniques. Neither the stoichiometric constants nor the density coefficients *b* and *a* are related; instead, they must be calculated using specific processes or experimentation. The exponential *n* for temperature specifies an extra temperature dependency of the reaction rate. In many circumstances, the dependency may be described as a single exponential term (with n = 0) since many fundamental interactions demonstrate Arrhenius behavior for minor temperature changes [55]. Moreover, under gasification or combustion conditions, a non-Arrhenius response may be seen [56], necessitating the addition of the constant *-n*. Table 3 summarizes the kinetic parameters and reaction rates obtained from the given references.

2.3. Energy and exergy assessment

Thermal energy and exergy are two important aspects to consider when examining and measuring the efficiency of a system. The exergy analysis approach is used to assess the effectiveness of a system in terms of energy quality and system efficiency. Exergy of a system is comprised of chemical exergy, potential exergy, physical exergy, and kinetic exergy. Potential and kinetic exergy are often disregarded in gasifier systems owing to the slight variations in velocity and elevation that occur throughout the gasification process [80]. In the majority of circumstances, the total physiochemical exergy of a material stream may be utilized to compute the total exergy available in the stream. Aside from this, the LHV is used mostly to assess the amount of usable fuel energy. Therefore, determining the LHV and exergy of the syngas produced during the gasification process is critical. Aspen Plus's list of stream characteristics include the LHV and physical exergy values of syngas, but the chemical exergy value must be determined explicitly. Values for the energy (Eq. (2)) and physical exergy (Eq. (3)) of material streams are calculated as follows:

$$e_{stream} = m(h - h_0) \tag{2}$$

$$\varepsilon_{ph} = \Delta h - T_0 \Delta s = (h - h_0) - T_0(s - s_0) \tag{3}$$

where m is mass flow rate of the stream, h is the specific enthalpy, h_0 is the specific enthalpy at ambient conditions, s is the specific entropy, s_0 is the specific entropy at ambient conditions, and T_0 is the ambient temperature. Calculating chemical exergy requires first identifying the exergy of each individual system component. For this purpose, environmental factors such as temperature, pressure, and chemical compounds were determined. The chemical exergy calculation for a syngas with several ingredients is given by:

$$EX_{ch} = \sum y_i EX_{ch}^0 + RT_0 \sum y_i \ln(y_i) \tag{4}$$

where R is the universal constant for gases, T_0 is the standard temperature, y_i is the molar fraction of a gaseous component, and EX_{ch}^0 is the standard chemical exergy of a gaseous component [81].

2.4. Development of the circulating fluidized bed gasifier using Aspen plus

Through planning, management, development, and problem-solving, a more comprehensive knowledge of the whole process may assist to remove barriers and so improve the plant's economic power [82]. The circulating fluidized bed gasifier model is described in detail in this section. Aspen Plus includes a large library of physical attributes that can be utilized in simulations. It can, meanwhile, simulate solid-state operations [83]. The large database of thermodynamic properties, chemical processes, and reaction kinetics allows accurate estimate

Table 3
Chemical reactions and reaction rate expressions with references.

Reaction	Reaction rate	Ref.
$CO + H_2O \leftrightarrow CO_2 + H_2$	$k_f = 2.78x10^3$ [CO][H_2O]exp(-1.26x10^7/RT_g) $k_b = 9.59x10^4$ [CO_2][H_2]exp(-4.66x10^7/RT_g)	[57–59]
$CO + H_2O \leftrightarrow CO_2 + H_2$	$k_f = 2.75x10^9$ exp(-8.368x10^7/RT)[CO][H_2O] $k_b = 1.0x10^{11}$ exp(-1.205x10^8/RT)[CO_2][H_2]	[60]
$CO + H_2O \leftrightarrow CO_2 + H_2$	$k_f = 2780$ exp(-1.255x10^7/RT)[CO][H_2O] $k_b = 1.049x10^5$ exp(-4.557x10^7/RT)[CO_2][H_2]	[61]
$CO + H_2O \leftrightarrow CO_2 + H_2$	$r_f = 2.5x10^8$ exp(-16597/T_g)[CO][H_2O] $r_b = 9.43x10^9$ exp(-20563/T_g)[CO_2][H_2]	[62]
$CO + H_2O \leftrightarrow CO_2 + H_2$	$r_f = 7.68x10^{10}$ T_g exp(-36640/T_g)[CO]$^{0.5}$[H_2O] $r_b = 6.4x10^9$ T_g exp(-39260/T_g)[H_2]$^{0.5}$[CO_2]	[63]
$C + CO_2 \leftrightarrow 2CO$	$k_{CO2} = 8.30x10^0$ T_p exp(-4.37x10^7/RT_p)	[64,65]
$C + CO_2 \leftrightarrow 2CO$	$r_f = 1.272$ T_s exp(-22645/T_s)[CO_2]	[63]
$C + CO_2 \leftrightarrow 2CO$	$r = 3.42$ T_s exp(-129700/R_uT_s)	[66]
$C + CO_2 \leftrightarrow 2CO$	$r = 9.1x10^6$ exp(-166000/R_uT_i)	[67,68]
$C + CO_2 \leftrightarrow 2CO$	$r_{CO2} = 342$ T exp(-15600/T)[CO_2]	[61]
$C + CO_2 \leftrightarrow 2CO$	$r = 36.16$ exp(-77.39/RT)	[69]
$C + H_2O \leftrightarrow CO + H_2$	$k_{H2O} = 4.56x10^1$ T_p exp(-4.37x10^7/RT_p)	[64,65]
$C + H_2O \leftrightarrow CO + H_2$	$r = 1.517x10^4$ exp(-121.62/RT)	[69]
$C + H_2O \leftrightarrow CO + H_2$	$r_f = 1.272$ T_s exp(-22645/T_s)[H_2O]	[63]
$C + H_2O \leftrightarrow CO + H_2$	$r = 5.7114$ T_s exp(-129700/R_uT_s)	[66]
$C + H_2O \leftrightarrow CO + H_2$	$r = 1.71x10^7$ exp(-211000/R_uT_i)	[67,68]
$C + H_2O \leftrightarrow CO + H_2$	$r_{H2O} = 342$ T exp(-15600/T)[H_2O]	[61]
$H_2 + 0.5O_2 \rightarrow H_2O$	$r = 5.159x10^{15}$ exp(-3430/T_g)$T_g^{-1.5}$[O_2][H_2]$^{1.5}$	[70]
$H_2 + 0.5O_2 \rightarrow H_2O$	$k = 2.2x10^9$ exp(-1.09x10^5/RT) [O_2][H_2]	[57]
$H_2 + 0.5O_2 \rightarrow H_2O$	$r = 1.63x10^{11}$ $T_g^{1.5}$ exp(-3430/T_g)[O_2][H_2]$^{1.5}$	[63]
$H_2 + 0.5O_2 \rightarrow H_2O$	$r = 2.2x10^9$ exp(-13109/T_g)[O_2][H_2]	[62]
$H_2 + 0.5O_2 \rightarrow H_2O$	$r = 1.08x10^{13}$ exp(-125/RT_g)[O_2][H_2]	[57]
$H_2 + 0.5O_2 \rightarrow H_2O$	$r = 1.00x10^{14}$ exp(-42/RT)[O_2][H_2]	[71]
$CH_4 + 2O_2 \rightarrow CO_2 + 2H_2O$	$r = 3.552x10^{14}$ exp(-15700/T_g)T_g^1[CH_4][O_2]	[70]
$CH_4 + 2O_2 \rightarrow CO_2 + 2H_2O$	$r = 3.552x10^{11}$ T_g^1 exp(-15700/T_g)[CH_4][O_2]	[63]
$CH_4 + 2O_2 \rightarrow CO_2 + 2H_2O$	$r = 2.119x10^{11}$ T_g^1 exp(-24379/T_g)[CH_4]$^{0.2}$[O_2]$^{1.3}$	[62]
$CH_4 + 2O_2 \rightarrow CO_2 + 2H_2O$	$r_{CH4} = 5.16x10^{13}$ T^{-1} exp(-130/T_g)[CH_4][O_2]	[72]
$CO + 0.5O_2 \rightarrow CO_2$	$r_{CO} = 2.32x10^{12}$ exp(-167/RT)[CO]^1[O_2]$^{0.25}$[H_2O]$^{0.5}$	[73]
$CO + 0.5O_2 \rightarrow CO_2$	$r_{CO} = 1.30x10^{11}$ exp(-126/RT)[CO]^1[O_2]$^{0.5}$[H_2O]$^{0.5}$	[74]
$CO + 0.5O_2 \rightarrow CO_2$	$r_{CO} = 4.78x10^8$ exp(-66.9/RT)[CO]^1[O_2]$^{0.3}$[H_2O]$^{0.5}$	[75]
$CO + 0.5O_2 \rightarrow CO_2$	$r_{CO} = 1.28x10^{17}$ exp(-289/RT)[CO]^1[O_2]$^{0.25}$[H_2O]$^{0.5}$	[76]
$CO + 0.5O_2 \rightarrow CO_2$	$r_{CO} = 3.25x10^{10}$ exp(-126/RT)[CO]^1[O_2]$^{0.5}$[H_2O]$^{0.5}$	[77]
$CO + 0.5O_2 \rightarrow CO_2$	$r = 1.0x10^{15}$ exp(-16000/T_g)[CO][O_2]$^{0.5}$	[70]
$CO + 0.5O_2 \rightarrow CO_2$	$k = 2.239x10^{12}$ exp(-1.67x10^5/RT)[CO][O_2]$^{0.25}$	[57]
$CO + 0.5O_2 \rightarrow CO_2$	$r = 5.62x10^{12}$ exp(-16000/T_g)[CO][O_2]$^{0.5}$	[63]
$CO + 0.5O_2 \rightarrow CO_2$	$r = 1.0x10^{10}$ exp(-15154/T_g)[CO][O_2]$^{0.5}$[H_2O]$^{0.5}$	[62]
$CO + 0.5O_2 \rightarrow CO_2$	$r = 1.78x10^{14}$ exp(-133/RT_g)[CO][O_2]$^{0.5}$	[78]
$CH_4 + H_2O \leftrightarrow CO + 3H_2$	$r = 3x10^5$ exp(-15042/T_g)[CH_4][H_2O]	[63]
$CH_4 + H_2O \leftrightarrow CO + 3H_2$	$r = 0.312$ exp(-15098/T_g)[CH_4][H_2O]	[62]
$CH_4 + H_2O \leftrightarrow CO + 3H_2$	$r_{CH4} = 3.00x10^8$ exp(-125/RT)[CH_4][H_2O]	[79]
$CH_4 + H_2O \leftrightarrow CO + 3H_2$	$r_{CH4} = 30$ exp(-1.247x10^8/RT)[CH_4][H_2O]	[61]
$CH_4 + H_2O \leftrightarrow CO + 3H_2$	$r = 7.301x10^{-2}$ exp(-36.15/RT)	[69]
$C + 0.5O_2 \rightarrow CO$	$r = 0.046x10^7$ exp(-13523/R_uT_i)	[67,68]
$C + 2H_2 \leftrightarrow CH_4$	$r_{H2} = 0.342$ T exp(-15600/T)[H_2]	[61]
$C + 2H_2 \leftrightarrow CH_4$	$r = 4.189x10^{-3}$ exp(-19.21/RT)	[69]

of process variables and features. Specifying the chemical compositions and detailing the flowchart with energy and material streams and unit operators are required to run the simulation.

In this study, kinetic modeling was applied using Aspen Plus v11 simulation software to depict the gasification process. Process streams in the Aspen Plus include mass and energy flows. Conventional, mixed, and non-conventional are the three types of material streams. As a fluid package, the Soave-Redlich-Kwong equation of state is used. During the design of the circulating fluidized bed gasifier, certain assumptions are taken into account:

- Ash is assumed to be inert.
- With no alterations in any of the variables throughout time, the gasifier system is in a steady state.
- The gasification system is isothermal.
- There is no pressure fluctuation in the unit blocks.
- In the unit blocks, there are no heat losses.
- The production of tar is disregarded.
- Since the gasifier model is one-dimensional, all changes in parameters are only examined in the axial direction.
- H_2, CH_4, N_2, CO_2, H_2O, and CO gases are present in the syngas.
- In the simulation, a power law kinetic equation is used.

Fig. 2 depicts the Aspen Plus flowsheet chart of the circulating fluidized bed gasification system proposed in this work.

The *FEEDSTCK* feedstock material was given an unconventional stream. The proximate and ultimate analyses of the solid fuel sample were included as component attributes of the stream *FEEDSTCK*. Following the classification of the fuel sample as a nonconventional component based on its elemental composition and proximate analysis results, the fuel's thermodynamic characteristics and flow rate were submitted. The feedstock must be converted into a structure that can be utilized to conduct the operations. For this purpose, the *DECOMP* block (RYield reactor) receives the *FEEDSTCK* stream and converts non-conventional substances into conventional chemicals. The fuel sample must be introduced dry, but the fuel entering the unit block must have the same amount of water as when it was first received. Consequently, using the *FEEDSTCK* moisture content previously determined in the proximate analysis, the calculator module was executed to determine the transition of dry basis elemental composition to as received basis in the *DECOMP* reactor. Using an external Fortran computation, the yield distribution was determined and supplied to the *DECOMP* unit block. In addition, the mixed stream *AGENT* was introduced to the system at atmospheric pressure. Before entering the gasifier, the feedstock material and the gasifying agent are mixed in the *MIXER* unit block. In this investigation, the *GASIFIER* RPlug unit block is employed to carry out the gasification processes. RPlug is a thorough simulation of plug flow reactors. In the RPlug process, complete radial blending is expected, but no axial blending is assumed. Additionally, RPlug may be used to model reactors with several thermal fluid streams (countercurrent or co-current). RPlug can manage kinetic processes, such as solid-state reactions. When using an RPlug to model a reactor, the user must define the reaction kinetics. Either the built-in reaction models or a user-defined Fortran routine may be used to provide reaction kinetics. In addition, a user can specify reactor type, operating conditions, and heat transfer parameters in the RPlug module, along with reactor dimensions, number of reactor tubes and phases to consider in the process and thermal fluid streams, which phases are placed in each product stream, reaction sets that describe the reactions to be included in the RPlug calculations, pressure at the reactor inlet and pressure drop across the reactor, details on the solid catalyst (if present), and reaction sets that describe the reactions to be included in the RPlug calculations. The obtained producer gas *PRODGAS* is then delivered to the *CLEANER* block, where the undesirable chemicals are removed and syngas *SYNGAS* is produced on the required basis.

2.5. The artificial neural network methodology

In recent years, as a consequence of advancements in machines and algorithms, ANNs have been used widely for predicting the system's behavior. ANNs are classified as computing systems. An ANN is composed of perceptrons, which are several single cells coupled by weights. A neuron's axon functions as the input layer, while the hidden layer is based on the accuracy of predicting and the output axon displays the results [84]. Signals entering the system are evaluated by the input layer. The information is sent from the input level to the weighted connections of the structure, where it is formed by several hidden layers of perceptrons at the output level. As input, each hidden neuron obtains weighted information from the level before. The mathematical model of a perceptron is demonstrated in Fig. 3.

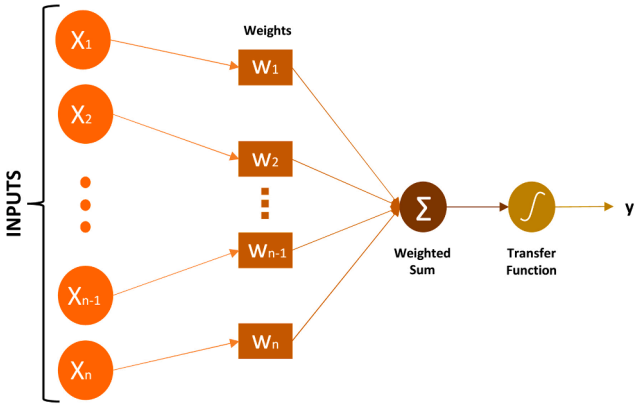

Fig. 3. The architecture of an artificial neuron (perceptron).

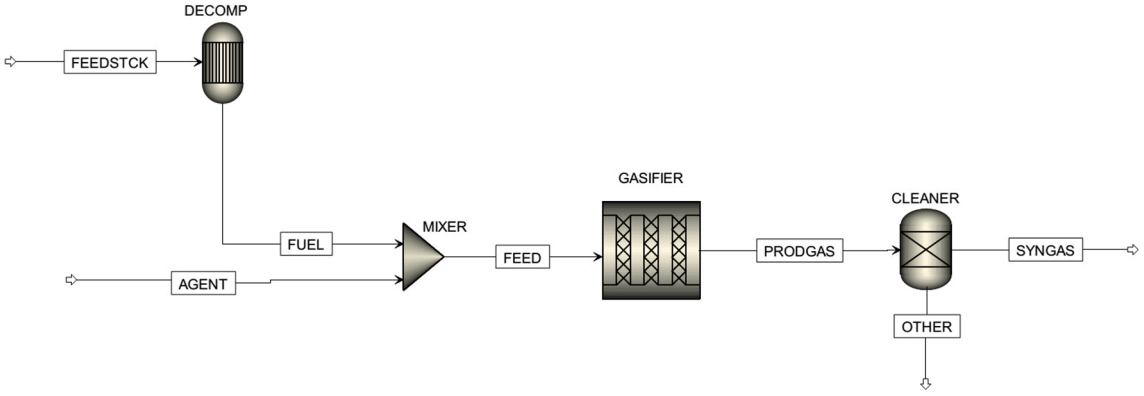

Fig. 2. Aspen Plus flowsheet diagram of the circulating fluidized bed gasifier model.

To calculate the output signal y, first the input signal x_i is multiplied by the weight w_i, and then add the bias value b_j to the resultant. Weights and biases are assigned at random, and weights are organized based on the difference in deviation among input and output. The following equation depicts the output of an artificial neuron [85]:

$$y = f\left(\sum_{i-1} w_{ji} x_i + b_j\right) \tag{5}$$

where f is the activation (transfer) function, and transfer function selection is critical for the learning process. Frequently, logarithmic and tangent sigmoid functions are used for this purpose. In this work, the tangent sigmoid function is chosen as the activation function:

$$f(x) = \frac{e^x - e^{-x}}{e^x + e^{-x}} \tag{6}$$

The two major features of ANN training are the forward propagation of knowledge and the reverse propagation of error. The transmission of information in the forward direction has been previously considered. After the data has been propagated forward, the global error is computed, and if it is greater than the objective error, the error is propagated backward to modify the biases and weights of each layer. The back propagation of the error is calculated as follows:

$$E = \frac{1}{2}\sum_{i=1}^{n} (y_i^d - y_i^p)^2 \tag{7}$$

$$w_{ij}(k+1) = w_{ij}(k) - \eta \frac{\partial E(k)}{\partial w_{ij}(k)} \tag{8}$$

$$b_{ij}(k+1) = b_{ij}(k) - \eta \frac{\partial E(k)}{\partial b_{ij}(k)} \tag{9}$$

where y_i^d is the ANN's expected output, y_i^p is the ANN's output, E is the global error, η is the learning rate, $b_{ij}(k)$ and $w_{ij}(k)$ are the k-th iteration's connection biases and weights across layers, respectively.

An ANN model does not memorize the input and output values of the network, but it does develop a relationship between them. The Levenberg-Marquardt algorithm [86] is the optimization function in this paper. This method also goes by the term damped least-squares technique. In the 1940s, Kenneth Levenberg first introduced the concept, and Donald Marquardt subsequently rediscovered it. This approach is often used in ANN learning operations. Levenberg-Marquardt is helpful when the ANN has large data sets since it may minimize memory space [87]. Levenberg-Marquardt is more favorable than other learning algorithms due to its stability and high convergence speed. When the damping coefficient is small, the Gauss-Newton technique is utilized, and when it is large, the gradient descent approach is used. Hence, the Levenberg-Marquardt approach may be used to obtain a global optimum [88].

If d is the objective value vector for m pieces of data and y is the fitting function's output vector, L is defined as [89]:

$$L = \sum_{j=1}^{m} (d_j - y_j)^2 \tag{10}$$

The update is as follows, according to the gradient descent method:

$$\Delta w_t = aJ^T W(d - y) \tag{11}$$

The Jacobian matrix of $\frac{\partial y}{\partial w_t}$ is written as J, while the weight vector is denoted by W. The update, according to the Gauss–Newton method, is as follows:

$$\Delta w_t = \left(J^T WJ\right)^{-1} J^T W(d - y) \tag{12}$$

The update rule is as follows, since Levenberg-Marquardt combines these approaches:

$$\Delta w_t = \left(J^T WJ + \lambda I\right)^{-1} J^T W(d - y) \tag{13}$$

where the identity matrix is denoted as I, while the damping factor is written as λ. If the updated parameter causes better progress than the old one, the new model parameters are accepted, and λ is reduced. Instead, the updated parameter set will be refused, and the value of λ will be raised [90].

3. Results and discussions

3.1. Model validation procedure of circulating fluidized bed gasifier

Model validation is essential immediately after model construction. Before doing the parametric analysis, it is necessary to verify the circulating fluidized bed gasifier model. Because a problematic model cannot be evaluated and appropriate conclusions cannot be formed. Using input parameters such as gasifier pressure and temperature, ultimate and proximate analysis results of feedstock material, type of gasification agent, and flow rates of inlet variables, the gasification procedures were simulated under the same circumstances as in experimental researches. In this kinetic modeling study, validation processes were conducted using seven different circulating fluidized bed gasifiers with various characteristics. Due to the fact that each experimental study has a unique reactor design, operating circumstances, fuel, etc., the kinetic parameters determined in the validation approach for each experiment are unique. The operating condition and gasifier size information for the experimental studies selected for the validation procedure are listed in Table 4.

When evaluating the parameters of the experimental investigations selected for validation, it is possible to infer that, with a few exceptions, they often have comparable characteristics. Aside from the sawdust and eucalyptus wood gasification processes, the lengths of the gasifiers are roughly 600 cm. Apart from the miscanthus pellet and subbituminous sample gasification processes, the diameters of the gasifiers range between 15 and 20 cm. However, the feedstock flow rate and air flow rate are drastically different. Despite the fact that this variation influences the ER, the ER values remain between 0.25 and 0.35, indicating that char conversion is optimal [91]. In addition, the gasifier temperatures are observed to be quite similar, at around 800 °C. The syngas compositions were compared after the simulation was run under the identical operating parameters as the experiments, and the results are summarized in Table 5. Quantitative measurement results such as relative error (RE), absolute error (AE), and mean absolute error (MAE) are also listed in the table for convenience of understanding of the comparison data.

$$Relative\ \ Error(\%) = \frac{(Predicted\ \ value - Actual\ \ value)}{Actual\ \ value} x100 \tag{14}$$

$$Absolute\ \ Error = |Predicted\ \ value - Actual\ \ value| \tag{15}$$

$$Mean\ \ Absolute\ \ Error = \frac{\sum_{i=1}^{n} |Predicted\ \ value_i - Actual\ \ value_i|}{n} \tag{16}$$

According to the comparison data, the model performs well even if the syngas compositions vary slightly. These variances are within the acceptable range. Despite many model assumptions, such as one-dimensional movement along the horizontal axis, neglection of particle size effect, hydrodynamic neglection, absence of pressure fluctuations, etc. the model simulated the practical circulating fluidized bed gasification process adequately. Further, attempts have been made to describe the gasification process, a thermochemical phenomenon involving several complicated processes, using just eight or nine reactions. Such a decrease leads to discrepancies in syngas compositions in addition to model assumptions.

In experimental research, the percentage of components reported for the different basis and, thus, the concentration values supplied for the

Table 4
Operational condition and gasifier size information of the experimental studies in the validation process.

Feedstock Material	Fuel Flow Rate (kg/h)	Air Flow Rate (kg/h)	ER	Length (cm)	Diameter (cm)	Temperature (°C)
Olive oil waste	60	170	0.41	650	20	780
Miscanthus pellet	16.8	28.23	0.30	600	8.3	753
Willow	69	158	0.37	600	20	827
Sawdust	18.8	23.2	0.19	350	15.3	800
Juliflora chips	30	35.32	0.20	500	15.6	800
Eucalyptus wood	11.6	15.54	0.23	230	25	798
Subbituminous	26.4	68	0.37	630	10	810

Table 5
Comparison of the syngas compositions for experimental and simulation works.

Composition (mol. %)	Olive oil waste				
	Literature [46]	**Model**	**RE (%)**	**AE**	**MAE**
H_2	5.4	4.70	−12.96%	0.70	3.696%
CO	8.6	5.09	−40.81%	3.51	
CO_2	21.7	17.56	−19.08%	4.14	
CH_4	3.0	4.01	33.67%	1.01	
N_2	59.46	68.58	15.34%	9.12	
Composition (mol. %)	**Miscanthus pellets**				
	Literature [47]	**Model**	**RE (%)**	**AE**	**MAE**
H_2	6.00	6.31	5.17%	0.31	1.428%
CO	12.57	11.25	−10.50%	1.32	
CO_2	16.00	14.57	−8.94%	1.43	
CH_4	2.45	1.97	−19.59%	0.48	
N_2	62.22	65.82	5.79%	3.60	
Composition (mol. %)	**Willow**				
	Literature [48]	**Model**	**RE (%)**	**AE**	**MAE**
H_2	7.20	7.97	10.69%	0.77	2.217%
CO	9.40	8.16	−13.19%	1.24	
CO_2	17.10	15.69	−8.25%	1.41	
CH_4	3.30	3.15	−4.55%	0.15	
N_2	60.47	51.88	−14.21%	8.59	
H_2O	14.26	13.12	−7.99%	1.14	
Composition (mol. %)	**Sawdust**				
	Literature [49]	**Model**	**RE (%)**	**AE**	**MAE**
H_2	9.50	10.57	11.26%	1.07	0.937%
CO	17.90	16.52	−7.71%	1.38	
CO_2	12.15	11.05	−9.05%	1.10	
CH_4	3.25	3.45	6.15%	0.20	
Composition (mol. %)	**Juliflora chips**				
	Literature [50]	**Model**	**RE (%)**	**AE**	**MAE**
H_2	10.5	12.58	19.81%	2.08	1.837%
CO	26.5	23.41	−11.66%	3.09	
CO_2	7.5	5.43	−27.60%	2.07	
CH_4	3.0	2.89	−3.67%	0.11	
Composition (mol. %)	**Eucalyptus wood**				
	Literature [51]	**Model**	**RE (%)**	**AE**	**MAE**
H_2	6.7	7.73	15.37%	1.03	1.325%
CO	19.2	17.98	−6.35%	1.22	
CO_2	15.2	13.53	−10.99%	1.67	
CH_4	4.4	5.69	29.32%	1.29	
Composition (mol. %)	**Subbituminous**				
	Literature [52]	**Model**	**RE (%)**	**AE**	**MAE**
H_2	8.0	9.38	17.25%	1.38	0.74%
CO	10.2	9.55	−6.37%	0.65	
CO_2	15.7	15.77	0.45%	0.07	
CH_4	1.0	1.37	37.00%	0.37	
N_2	65.1	63.87	−1.89%	1.23	

syngas composition might vary. However, the concentrations of main syngas components such as H_2, CO, CO_2, and CH_4 are very consistent throughout all investigations. In addition, different quantitative error outcomes may be analyzed to determine the extent to which estimated values deviate from the actual results. The magnitude of divergence could therefore be assessed from several perspectives. The relative errors of CH_4 concentrations, for instance, are 37.00% and 19.59% for subbituminous and miscanthus pellets, respectively. The quantity of CH_4 in syngas is rather low, thus while the deviations seem substantial at first inspection, they are actually the outcome of very small differences. At this point, it is helpful to check for other quantitative error results. For this reason, the absolute error and the mean of the absolute error values are also included in the Table 5. In this study, the mean absolute errors for all validation series are below 4%. For some experimental validations, the mean absolute errors are even below 1%. Moreover, other researchers have also reported comparable deviations when comparing syngas compositions [19,92–96]. The deviations obtained in this study were similar or lower than those in the literature.

As mentioned earlier, each experimental validation study varies from the others in terms of operational and design differences. Thus, the kinetic parameters for each validation step vary. Table 6 lists the modified kinetic parameters for the validation process.

As demonstrated in Table 6, the kinetic parameters are significantly dependent on the operating circumstances. During the process of modification, on the other hand, care was taken not to significantly alter the driving force, temperature exponent, and relative activation energy parameters. In general, the pre-exponential factor value was changed to provide a composition equivalent to the syngas composition achieved in the experimental research. Thus, the optimization procedure was used to increase or decrease the formation of the desired component.

3.2. Parametric study

Using the sensitivity analysis module, the effect of independent factors and dependent variables was investigated. As input variables, the air-to-fuel ratio, gasifier temperature, and gasifier length and diameter were selected. Due to the fact that operational parameters have equivalent impacts on feedstock materials, only the Juliflora chips sample is displayed to prevent the plots from becoming too cluttered. Table 7 lists the boundary conditions for the parametric analysis procedure in Juliflora chips gasification.

The sample of Juliflora chips was not exceptional; other feedstock materials were subject to the same boundary constraints. The gasifier's temperature was varied between 750 and 850 °C, the length of the gasifier was varied between −100 and +100 cm, the diameter of the gasifier was varied between −5 and +5 cm, and the air/fuel ratio was changed between 0.15 and 0.50. Syngas composition, syngas LHV and syngas exergy (sum of chemical and physical) were analyzed as dependent variables.

3.2.1. Effect of the gasifier temperature

The temperature of the gasifier is one of the most influential parameters on the composition and properties of syngas. The most of endothermic equilibrium activities are significantly influenced by the temperature. The effect of gasifier temperature on syngas content is

Table 6
The modified kinetic parameters for the validation process.

Reaction	Olive oil waste			
	k	**T^n**	**Ea**	**Driving force**
$C + H_2O \leftrightarrow CO + H_2$	342	1	1.3329e + 08 J/kmol	$[H_2O]$
$C + 2H_2 \leftrightarrow CH_4$	0.342	1	5.7e + 07 J/kmol	$[H_2]$
$C + CO_2 \leftrightarrow 2CO$	342	1	1.306984e + 08 J/kmol	$[CO_2]$
$CH_4 + H_2O \leftrightarrow CO + 3H_2$	30	0	1.247e + 08 J/kmol	$[CH_4]$ $[H_2O]$
$CO + H_2O \leftrightarrow CO_2 + H_2$	2780	0	2.135e + 07 J/kmol	$[CO]$ $[H_2O]$
$CH_4 + 2O_2 \rightarrow CO_2 + 2H_2O$	3.98e + 11	0	1.67e + 10 kcal/mol	$[CH_4]^{0.7}$ $[O_2]^{0.8}$
$2CO + O_2 \rightarrow 2CO_2$	3.98e + 11	0	1.67e + 11 J/kmol	$[CO]$ $[O_2]^{0.25}$ $[H_2O]^{0.5}$
$C + O_2 \rightarrow CO_2$	5.67e + 08	0	1.5e + 08 J/kmol	$[O_2]$
$H_2 + 0.5O_2 \rightarrow H_2O$	1.08e + 09	0	100 kJ/mol	$[H_2]$ $[O_2]$
Reaction	**Miscanthus pellets**			
	k	**T^n**	**Ea**	**Driving force**
$C + H_2O \leftrightarrow CO + H_2$	342	1	1.296984e + 08 J/kmol	$[H_2O]$
$CO + H_2O \leftrightarrow CO_2 + H_2$	0.01278	0	1.26e + 07 J/kmol	$[CO]$ $[H_2O]$
$C + CO_2 \leftrightarrow 2CO$	1.10e + 09	0	1.88e + 08 J/kmol	$[CO_2]$
$C + 2H_2 \leftrightarrow CH_4$	900.42	1	1.296984e + 08 J/kmol	$[H_2]$
$H_2 + 0.5O_2 \rightarrow H_2O$	94,300	0	3.05e + 07 J/kmol	$[H_2]$ $[O_2]$
$CO + 0.5O_2 \rightarrow CO_2$	0.33	0	126 kJ/mol	$[CO]$ $[O_2]^{0.5}$ $[H_2O]^{0.5}$
$C + O_2 \rightarrow CO_2$	6.00e + 07	0	38200 kcal/kmol	$[O_2]^{0.78}$
$C + 0.5O_2 \rightarrow CO$	0.3	1	92300 kJ/kmol	$[O_2]^{0.4}$
Reaction	**Willow**			
	k	**T^n**	**Ea**	**Driving force**
$C + H_2O \leftrightarrow CO + H_2$	142	1	1.296984e + 08 J/kmol	$[H_2O]$
$CO + H_2O \leftrightarrow CO_2 + H_2$	12.78	0	1.26e + 07 J/kmol	$[CO]$ $[H_2O]$
$C + CO_2 \leftrightarrow 2CO$	7.00e + 07	0	1.88e + 08 J/kmol	$[CO_2]$
$C + 2H_2 \leftrightarrow CH_4$	398.42	1	1.296984e + 08 J/kmol	$[H_2]$
$H_2 + 0.5O_2 \rightarrow H_2O$	15543.53	0	3.05e + 07 J/kmol	$[H_2]$ $[O_2]$
$CO + 0.5O_2 \rightarrow CO_2$	0.0033	0	126 kJ/mol	$[CO]$ $[O_2]^{0.5}$ $[H_2O]^{0.5}$
$C + O_2 \rightarrow CO_2$	2.00e + 07	0	38200 kcal/kmol	$[O_2]^{0.78}$
$C + 0.5O_2 \rightarrow CO$	0.28	1	92300 kJ/kmol	$[O_2]^{0.4}$
Reaction	**Sawdust**			
	k	**T^n**	**Ea**	**Driving force**
$C + H_2O \leftrightarrow CO + H_2$	342	1	1.296984e + 08 J/kmol	$[H_2O]$
$CO + H_2O \leftrightarrow CO_2 + H_2$	242.78	0	1.26e + 07 J/kmol	$[CO]$ $[H_2O]$
$C + CO_2 \leftrightarrow 2CO$	50,000	0	1.88e + 08 J/kmol	$[CO_2]$
$C + 2H_2 \leftrightarrow CH_4$	356	1	1.296984e + 08 J/kmol	$[H_2]$
$H_2 + 0.5O_2 \rightarrow H_2O$	36,430	0	3.05e + 07 J/kmol	$[H_2]$ $[O_2]$
$CO + 0.5O_2 \rightarrow CO_2$	0.0033	0	126 kJ/mol	$[CO]$ $[O_2]^{0.5}$ $[H_2O]^{0.5}$
$C + O_2 \rightarrow CO_2$	1.20e + 07	0	38200 kcal/kmol	$[O_2]^{0.78}$
$C + 0.5O_2 \rightarrow CO$	0.58	1	92300 kJ/kmol	$[O_2]^{0.4}$
Reaction	**Juliflora chips**			
	k	**T^n**	**Ea**	**Driving force**
$C + H_2O \leftrightarrow CO + H_2$	142.00	1	1.296984e + 08 J/kmol	$[H_2O]$
$CO + H_2O \leftrightarrow CO_2 + H_2$	12.78	0	1.26e + 07 J/kmol	$[CO]$ $[H_2O]$
$C + CO_2 \leftrightarrow 2CO$	50000.00	0	1.88e + 08 J/kmol	$[CO_2]$
$C + 2H_2 \leftrightarrow CH_4$	226.42	1	1.296984e + 08 J/kmol	$[H_2]$
$H_2 + 0.5O_2 \rightarrow H_2O$	17000.00	0	3.05e + 07 J/kmol	$[H_2]$ $[O_2]$
$CO + 0.5O_2 \rightarrow CO_2$	7.00e + 07	0	126 kJ/mol	$[CO]$ $[O_2]^{0.5}$ $[H_2O]^{0.5}$
$C + O_2 \rightarrow CO_2$	6.00e + 06	0	38200 kcal/kmol	$[O_2]^{0.78}$
$C + 0.5O_2 \rightarrow CO$	1.10	1	92300 kJ/kmol	$[O_2]^{0.4}$
Reaction	**Eucalyptus wood**			
	k	**T^n**	**Ea**	**Driving force**
$C + H_2O \leftrightarrow CO + H_2$	0.342	1	1.296984e + 08 J/kmol	$[H_2O]$
$CO + H_2O \leftrightarrow CO_2 + H_2$	62.78	0	1.26e + 07 J/kmol	$[CO]$ $[H_2O]$
$C + CO_2 \leftrightarrow 2CO$	5000	0	1.88e + 08 J/kmol	$[CO_2]$
$C + 2H_2 \leftrightarrow CH_4$	250	1	1.296984e + 08 J/kmol	$[H_2]$
$H_2 + 0.5O_2 \rightarrow H_2O$	25543.53	0	3.05e + 07 J/kmol	$[H_2]$ $[O_2]$
$CO + 0.5O_2 \rightarrow CO_2$	3.90e + 07	0	126 kJ/mol	$[CO]$ $[O_2]^{0.5}$ $[H_2O]^{0.5}$
$C + O_2 \rightarrow CO_2$	6.00e + 06	0	38200 kcal/kmol	$[O_2]^{0.78}$
$C + 0.5O_2 \rightarrow CO$	0.38	1	92300 kJ/kmol	$[O_2]^{0.4}$
Reaction	**Subbituminous**			
	k	**T^n**	**Ea**	**Driving force**
$C + H_2O \leftrightarrow CO + H_2$	342	1	1.296984e + 08 J/kmol	$[H_2O]$
$CO + H_2O \leftrightarrow CO_2 + H_2$	102.78	0	1.26e + 07 J/kmol	$[CO]$ $[H_2O]$
$C + CO_2 \leftrightarrow 2CO$	5.00e + 07	0	1.88e + 08 J/kmol	$[CO_2]$
$C + 2H_2 \leftrightarrow CH_4$	206.42	1	1.296984e + 08 J/kmol	$[H_2]$
$H_2 + 0.5O_2 \rightarrow H_2O$	7043.53	0	3.05e + 07 J/kmol	$[H_2]$ $[O_2]$
$CO + 0.5O_2 \rightarrow CO_2$	0.0033	0	126 kJ/mol	$[CO]$ $[O_2]^{0.5}$ $[H_2O]^{0.5}$
$C + O_2 \rightarrow CO_2$	3.00e + 07	0	38200 kcal/kmol	$[O_2]^{0.78}$
$C + 0.5O_2 \rightarrow CO$	0.6	1	92300 kJ/kmol	$[O_2]^{0.4}$

Table 7
Boundary conditions for the parametric analysis procedure in Juliflora chips gasification.

Independent variable	Minimum condition	Base case	Maximum condition
Temperature (°C)	750	820	850
Air/fuel ratio	0.15	0.50	0.50
Length (cm)	400	500	600
Diameter (cm)	10	15.6	20

given in Fig. 4.

At increased temperatures, the syngas composition chart reveals that the CO and H_2 concentrations increase while the H_2O concentration decreases. The CO concentration increased from 21.54% to 24.93%, the H_2 increased from 12.06% to 14.11%, and H_2O decreased from 24.88% to 15.55%. The increasing concentrations of CO and H_2 at high temperatures may be explained by the water–gas reaction, a vigorous heterogeneous endothermic process. Increased CO and H_2 formation at high temperatures has also been reported by other researchers [18,97,98]. In addition, the decrease in H_2O concentration is a result of the heterogeneous water–gas process. The rise in CO was substantial up to 800 °C, but afterwards it was moderate. In contrast, low levels of CH_4 and CO at high temperatures showed a slight rise. The rapid rise in CO concentration may have promoted CO_2 synthesis, despite the exothermic nature of the water–gas shift reaction. This is further supported by the fact that CO production decreases at high temperatures, although H_2O consumption stays constant. The composition of syngas, which varies with temperature, has an effect on its calorific value. The influence of gasifier temperature on syngas exergy and LHV is visualized in Fig. 5.

Between 750 and 850 °C, there was a steady rise in syngas exergy and

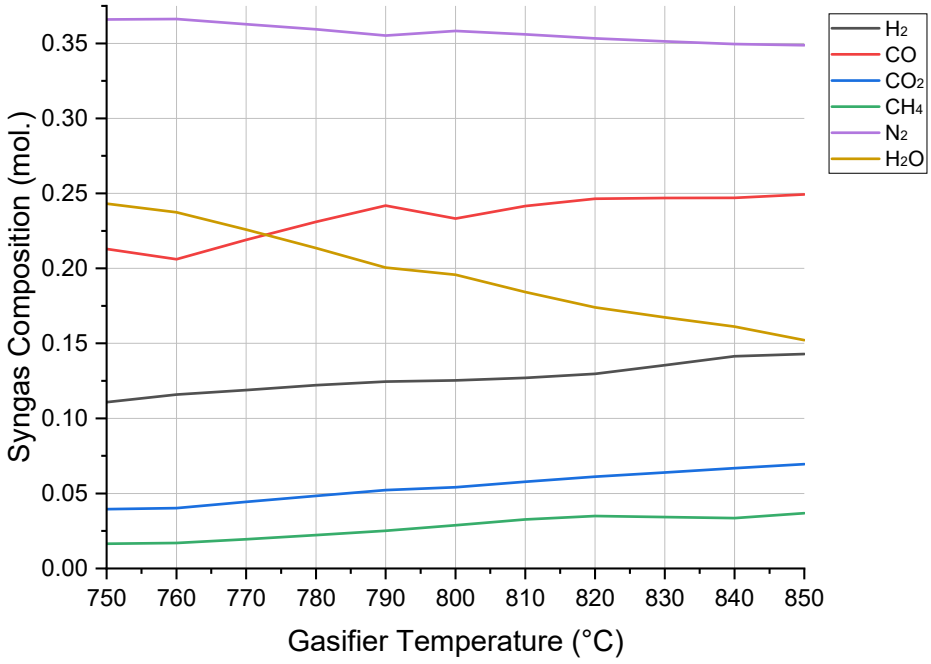

Fig. 4. Effect of gasifier temperature on syngas content.

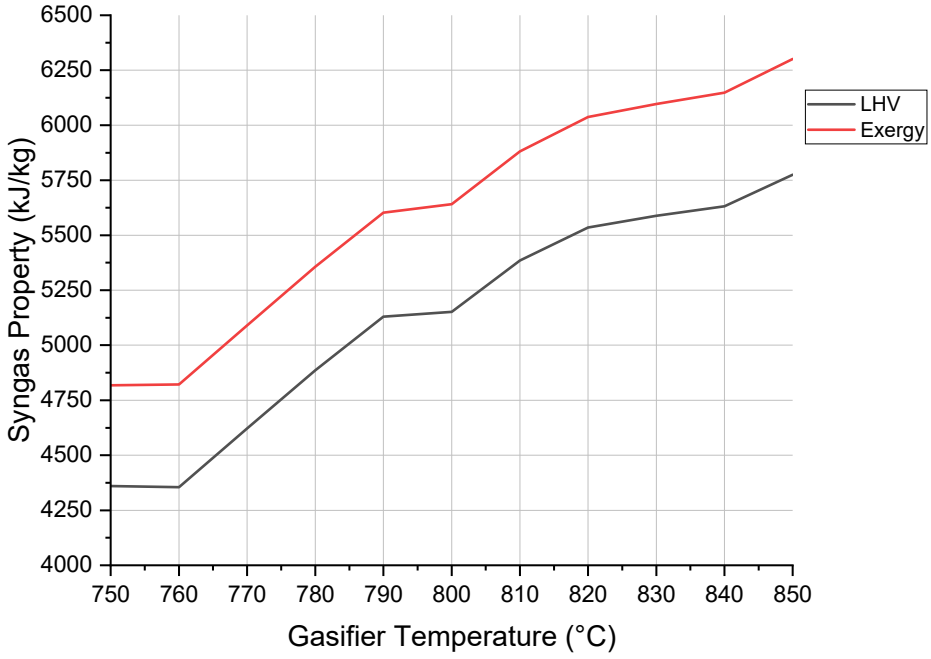

Fig. 5. Effect of gasifier temperature on syngas exergy and LHV.

LHV. Syngas exergy improved from 4817 to 6301 kJ/kg, whereas syngas LHV increased from 4360 to 5774 kJ/kg. Temperature-induced increments in CO and H_2 concentrations led to a rise in the LHV, despite a slight improvement in CO_2 concentration. In addition, the decrease in H_2O content caused by an increase in gasifier temperature improved syngas LHV. When operated at high temperatures, the gasifier provides hot gas products with improved functional capability. In addition, when the temperature increases, the composition of the gaseous product changes, which impacts its chemical exergy.

3.2.2. *Effect of the air/fuel ratio*

As the amount of gasifying agent supplied to the reactor varies, so does the concentration of the reactant. Consequently, gasification processes are changed, and the composition of syngas varies. In this work, the air-to-fuel ratio (kg/kg) was used as an independent variable to assess the influence of gasifying agent concentration. The effect of air/fuel ratio on syngas composition is demonstrated in Fig. 6.

As the amount of air in the gasifier grows, the amount of oxygen in the reactant rises, resulting in an acceleration of combustion processes. As a result, increasing the air-to-fuel ratio reduces the concentrations of CH_4, H_2 and CO. The H_2 decreased from 13.57% to 11.84%, CH_4 decreased from 16.52% to 10.88%, and CO decreased from 34.91% to 30.52%. Certainly, as the amount of air supplied to the reactor is increased, the concentration of N_2 in the syngas, as well as the

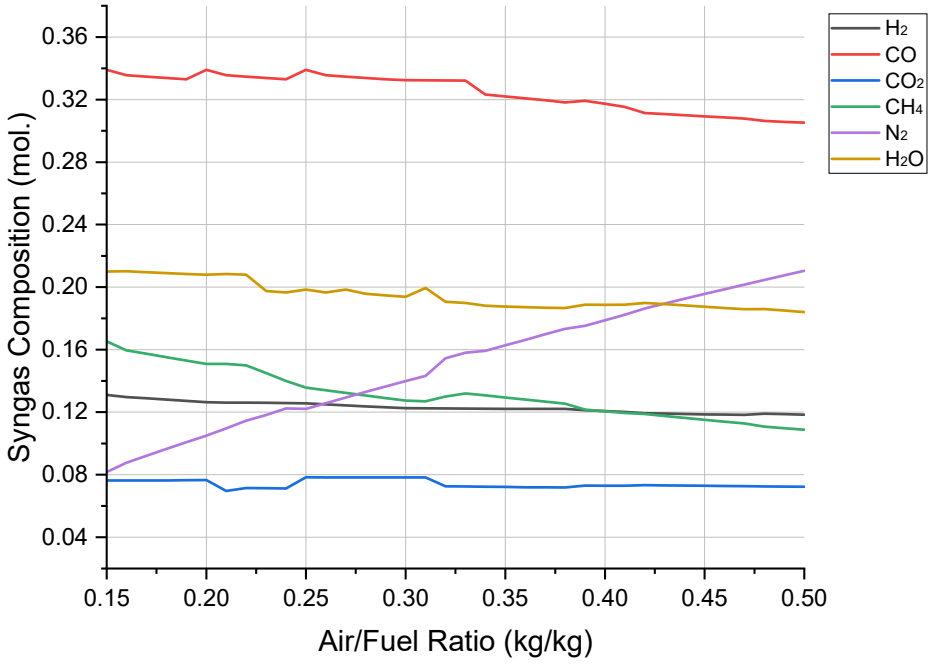

Fig. 6. Effect of air/fuel ratio on syngas content.

concentrations of combustion products CO_2 and H_2O, should increase. Thus, the N_2 concentration increased from 8.17% to 21.04%. On the other hand, the CO_2 content decreased slightly (from 7.22% to 6.99%), and the H_2O concentration decreased (from 21.11% to 18.40%). This demonstrates that heterogeneous processes continue to prevail in the gasifier. In water–gas and Boudouard reactions, the H_2O and CO_2 formed by combustion processes were consumed. The slight drop in H_2 and CO concentrations, which are predicted to decrease dramatically as a consequence of combustion operations, can also be addressed in terms of explaning this phenomenon. The decrease in CO and H_2 concentrations due to the increase of the amount of air fed to the reactor was also reported by other authors [68,69,99]. The impact of air/fuel ratio on syngas exergy and LHV is illustrated in Fig. 7.

A continuous decrease in exergy and LHV was observed with the increase of air/fuel ratio. Syngas exergy decreased from 12,678 to 9486 kJ/kg, and syngas LHV reduced from 11,814 to 8865 kJ/kg. Increasing the amount of air supplied to the gasifier has no beneficial impact on the concentration of any of the valuable gas species. In addition, the substantial increase in N_2 concentration dilutes syngas, resulting in a decline in quality. Syngas LHV, which decreased with increasing air supply to the reactor, was also reported by other researchers [32,96].

3.2.3. *Effect of gasifier length*

In addition to the operating circumstances, the gasifier design influences the qualities of the gas product to be produced, as previously described. As the length of the gasifier increases, the residence time of

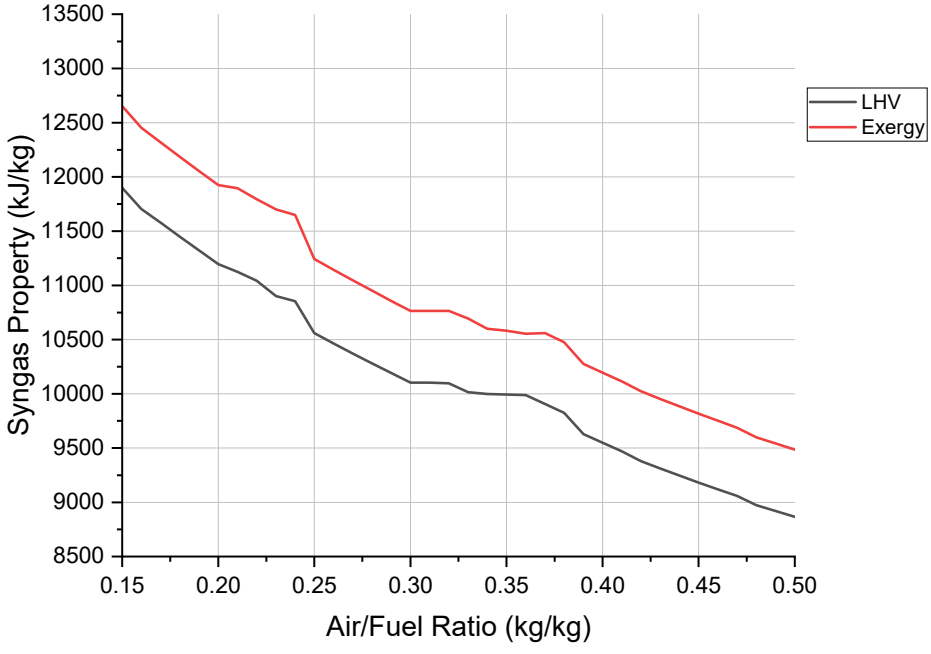

Fig. 7. Impact of air/fuel ratio on syngas exergy and LHV.

the reactants and products increases, affecting the equilibrium states of heterogeneous and homogeneous processes. The effect of gasifier length on syngas composition is given in Fig. 8.

While increasing the length of the gasifier increased the concentration of beneficial gases, it decreased the quantity of gas components that would deteriorate the quality of the syngas. The CO concentration increased from 23.92% to 24.84%, and CH_4 concentration increased from 3.17% to 3.61%. Further, the H_2O decreased from 18.17% to 17.01%, and N_2 decreased from 35.56% to 35.26%. The decrease in H_2O concentration and the rise in CO concentration may be explained by heterogeneous steam gasification processes. In addition, heterogeneous methanization processes may explain the increase in CH_4 concentration as the length of the gasifier increases. Increasing CO concentration with enlarged gasifier height [100], further, decreasing H_2O concentration and slightly changing CH_4 concentration with increasing gasifier height were also reported by other researchers [32,101]. The fact that H_2 does not increase as the gasifier length increases may be due to the suppression by the methanation process. It was also discovered that as the length of the gasifier expanded, the CO_2 concentration improved slightly. While the char combustion process can account for this, the non-violent growth can be attributed to the Boudouard reaction, which suppresses CO_2 formation. The influence of gasifier length on syngas exergy and LHV is shown in Fig. 9.

Extending the length of the gasifier, as anticipated, increased syngas exergy and LHV due to greater concentrations of valuable gases and lower quantities of N_2 and H_2O. Syngas exergy increased from 5876 to 6106 kJ/kg, and syngas LHV improved from 5370 to 5606 kJ/kg. Although the LHV and exergy curves have similar patterns, LHV has a lower value than exergy when evaluating just combustible components under the same operating conditions.

3.2.4. *Effect of gasifier diameter*

Similarly to the gasifier length, the gasifier diameter is a crucial dimension parameter. The diameter of the gasifier also has an effect on the residence time in the reactor and the equilibrium state of the processes. The effect of gasifier diameter on syngas composition is visualized in Fig. 10.

The CO concentration increased from 19.79% to 25.50%, the CH_4 concentration increased from 2.27% to 3.80%, and CO_2 concentration increased from 5.22% to 6.43%. Further, the H_2 decreased from 14.94% to 13.18%, and H_2O decreased from 18.65% to 16.11%. The H_2O decrement shows that the water–gas reaction becomes more dominant as the diameter of the gasifier increases. The rise in CH_4 concentration and decrease in H_2 concentration indicated that increasing the diameter of the gasifier promotes heterogeneous methanization processes. Expansion of the gasifier's diameter may result in an increase in CO_2 concentration as a result of the char combustion process. LHV and exergy values will undoubtedly change as the syngas content varies with increasing gasifier diameter. The influence of diameter on syngas properties is demonstrated in Fig. 11.

As predicted, increasing the diameter of the gasifier improved the LHV and exergy of syngas due to higher concentrations of favorable gaseous components and lower N_2 and H_2O quantities. Syngas exergy increased from 5351 to 6241 kJ/kg, and syngas LHV improved from 4844 to 5747 kJ/kg. Increment of syngas LHV with expanding reactor diameter has also been reported by other authors [100].

3.2.5. *Effect of operating parameters on carbon conversion*

Prior parametric investigations have shown that operational parameters have a substantial effect on the composition and calorific value of syngas. It has been observed that heterogeneous gasification processes have a significant role in the assessment of changes in the composition of syngas and, therefore, in the thermal quality. Particularly, the water–gas and methanization processes played a vital role in defining the syngas properties. In addition, when investigating variations in CO_2 content, it was observed that carbon combustion had a significant influence. Therefore, the impacts of operational and design factors on carbon conversion are discussed in this section. When examining the effect of an independent parameter for Juliflora chips gasification, other input variables are at the base case. The effects of operational and design parameters on carbon conversion are illustrated in Fig. 12.

On the superficial, it seems that a longer gasifier, a large gasifier diameter, and a high gasifier temperature all enhance carbon conversion. In contrast, while increasing the air-to-fuel ratio normally improves carbon conversion, its profile is more irregular than that of the other input parameters. The carbon conversion rose from 85.17% to 97.96% when the gasifier's length was enlarged from 4 m to 6 m. This is expected because solid carbon that is maintained in the reactor for long

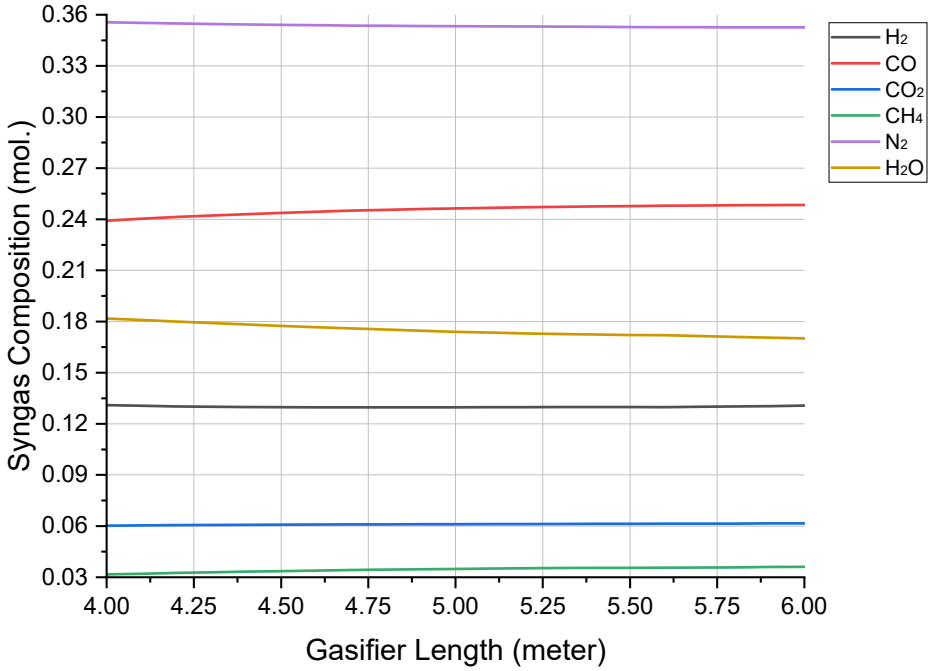

Fig. 8. Effect of gasifier length on syngas content.

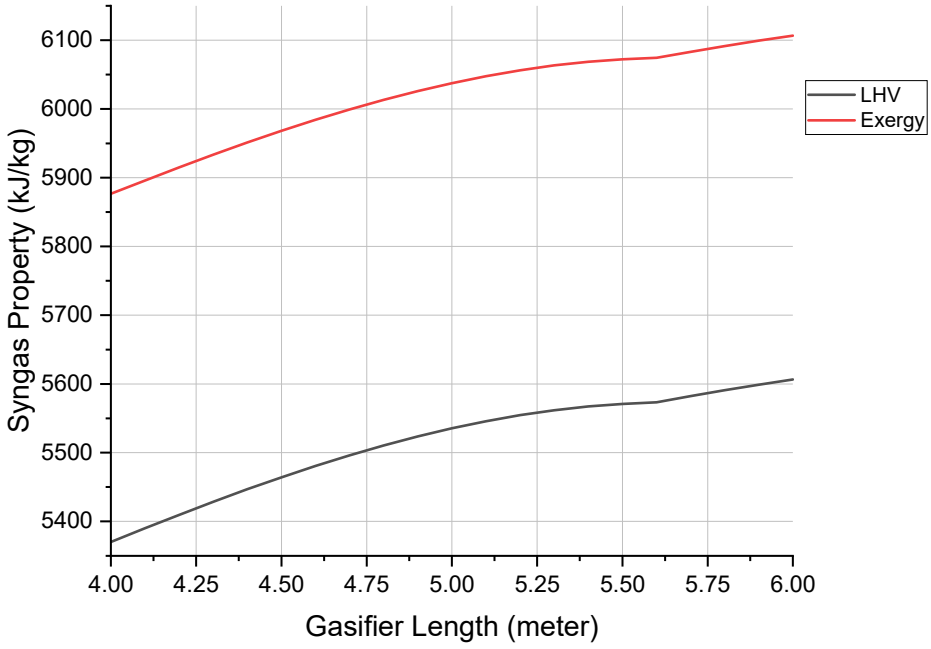

Fig. 9. Effect of gasifier length on syngas exergy and LHV.

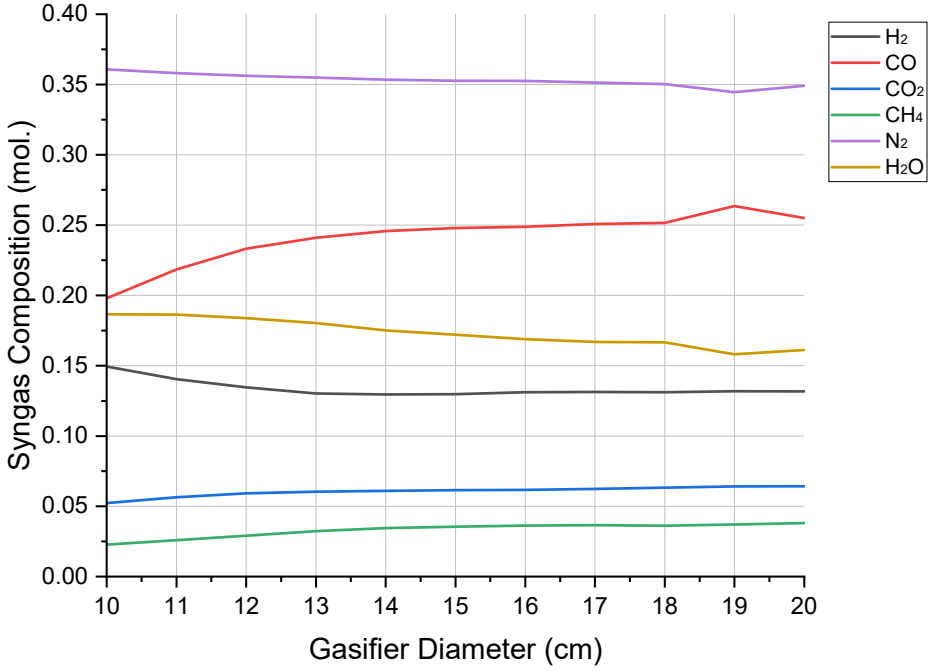

Fig. 10. Effect of gasifier diameter on syngas content.

periods of time reacts with the gaseous components and is consumed. The improved carbon conversion with increased gasifier length has also been reported by other authors [100]. The expanding gasifier diameter can be inferred in the same method. Carbon conversion improved from 63.90% to 97.96% when the gasifier diameter expanded from 15 cm to 20 cm. By analyzing this variance, it is possible to determine that the diameter of the gasifier is more relevant for carbon conversion than its length. The improved carbon conversion with increasing gasifier diameter has also been reported by other researchers [100]. The growing CO_2 and CO concentrations as the gasifier length rose, and the increasing CH_4, CO, and CO_2 concentrations as the gasifier diameter expanded, were explained by analyzing associated reactions. Increasing carbon conversion graphs with increasing gasifier diameter and length further confirmed the results obtained in the previous sections. Furthermore, the carbon conversion, which increases as the amount of air supplied to the gasifier increases, is quite rational. By boosting combustion processes with a considerable amount of oxidant added to the reactor, char formation was decreased. Complete combustion products H_2O and CO_2 enhanced carbon conversion through affecting the water–gas and Boudouard reactions, and indirectly the methanization process. As the air/fuel ratio increased from 0.15 to 0.50, the carbon conversion increased from 90.89% to 97.99%. The increased carbon conversion, which improves when the quantity of air blown to the reactor is increased, has also been mentioned by other authors

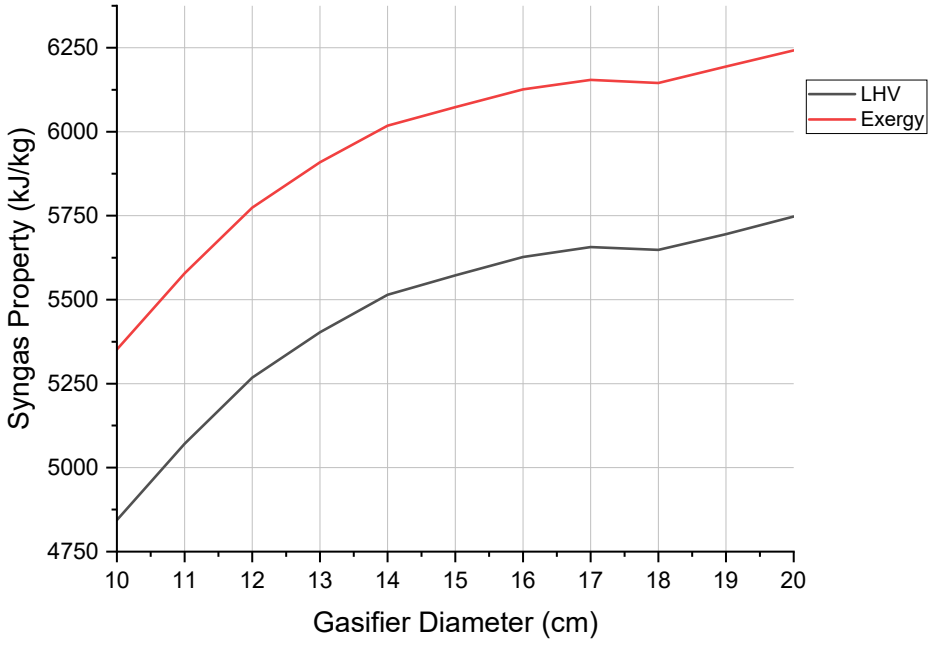

Fig. 11. Effect of gasifier diameter on syngas exergy and LHV.

[68,69,96]. The last independent variable, gasifier temperature, had a substantial effect on carbon conversion, which was possibly the most important variable. Carbon conversion improved from 54.57% to 98.07% when the gasifier temperature increased from 750 °C to 850 °C. Specifically, carbon conversion increases considerably over 810 °C. Increased carbon conversion at high temperatures can be attributed to mostly endothermic char gasification processes. Improved carbon conversion with increasing temperature has also been reported by other researchers [32,68,69,98].

3.3. A statistical analysis on the dataset created

The parametric investigations demonstrated that the operating parameters and gasifier design had a substantial effect on the overall system performance. To develop an adequate model, it is necessary to choose inputs from among the network parameters that have a significant effect. For seven different feedstock materials and gasifier design, a temperature rise of 10 °C was accounted for in the parametric study, an air/fuel ratio increase of of 0.01, a gasifier length increase of 10 cm, and gasifier diameter increase of 1 cm. As a result, a dataset containing 258,816 rows was created. Each row includes C, H, and O values of fuel sample, gasifier diameter and length, air/fuel ratio, and gasifier temperature as inputs; H_2, CH_4, CO and CO_2 concentrations, LHV and exergy values of syngas as outputs. A brief description of the parameters chosen in this work is listed in Table 8.

The average temperature of the gasifier was found to be 789.99 °C, with a mean air/fuel ratio of 0.33. The maximum and minimum numbers of the air/fuel ratio and gasifier temperature in the dataset are based on parametric studies' maximum and minimum values. This indicates that the dataset contains the whole spectrum of findings from the parametric tests. The H data revealed that the minimum and maximum values for the characteristics of the fuel samples were 3.46 and 6.59, respectively. 5.87 was determined to be the average H value. Furthermore, the average values for C and O were 48.27 and 39.63, respectively. The lowest and highest numbers of the parameters C, H, and O indicate that the dataset comprises all feedstock materials' outcomes. When the computed mean values for elemental composition are shown on the Van Krevelen diagram, this produced pseudo sample (H/C: 1.46 and O/C: 0.62) fits about in the middle of the biomass-specific zone. This is a reasonably predictable outcome given that six of the seven feedstock materials used in this investigation comprised of biomass. Comparing the maximum, lowest, and average values of LHV with exergy reveals that exergy is always greater than LHV. The fact that the standard deviations for LHV and exergy are so similar, 2603.42 and 2663.72, respectively, is further more evidence that these parameters behave similarly yet have different values.

Despite the fact that sensitivity analysis found a relationship between the output and input data sets, utilizing a heatmap to display the correlations is a practical and efficient method for examining the relationships. By using correlation matrix as a tool, Fig. 13 demonstrates the relationships between the components mentioned previously.

The intensity of the color and the diameter of the circles show the degree of association. There was a considerable negative correlation between C and H, as well as C and O. Subbituminous, for instance, is a carbon-rich solid fuel with a high degree of carbonization and a low proportion of hydrogen and oxygen. In contrast, H and O were shown to have a positive correlation. Since samples of biomass include a substantial quantity of volatile materials, oxygen and hydrogen concentrations are also high. Temperature, diameter, and length, which are additional input factors, show no significant negative or positive association with one another. The relationship between diameter and hydrogen is positive, while the relationship between length and oxygen is negative. For oxygen-rich fuels, shorter reactors are used, while longer gasifiers are required for carbon-rich fuels. When solid samples with a low carbon content are gasified in tall reactors, warnings or errors may occur because carbon conversion is finished early. Due to the removal of erroneous or warning data during the creation of the dataset, such a correlation may have been seen. In addition, when the relationship between fuel qualities and syngas composition is analyzed, a number of remarkable outcomes appear. Although there is no apparent relationship, as the carbon content of the fuel increases, the concentrations of H_2 and CO_2 in the syngas composition increase while the concentrations of CO decrease. In addition, when the H content of the fuel increases, the H_2 percentage in the syngas composition decreases while the CH_4 concentration increases. Increasing the concentration of oxygen in the fuel decreases the concentration of CO_2 in the syngas. In conclusion, when the degree of carbonization of solid fuel increases, the formation of H_2 and CO_2 increases owing to heterogeneous gasification processes. This is proved by the fact that high amounts of hydrogen and oxygen, which are similar in biomass samples, inhibit the synthesis of H_2 and CO_2. When

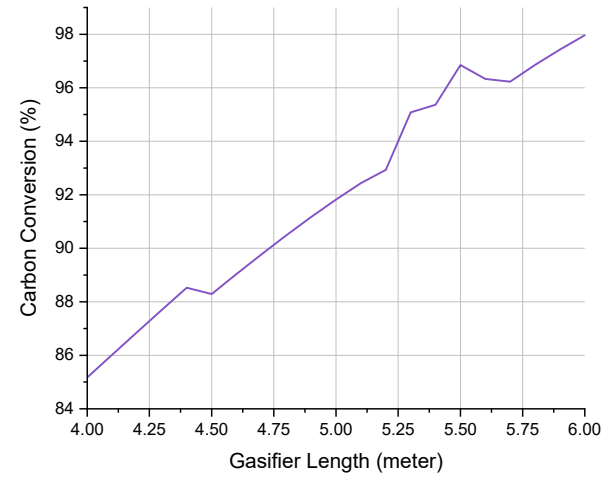

(a)

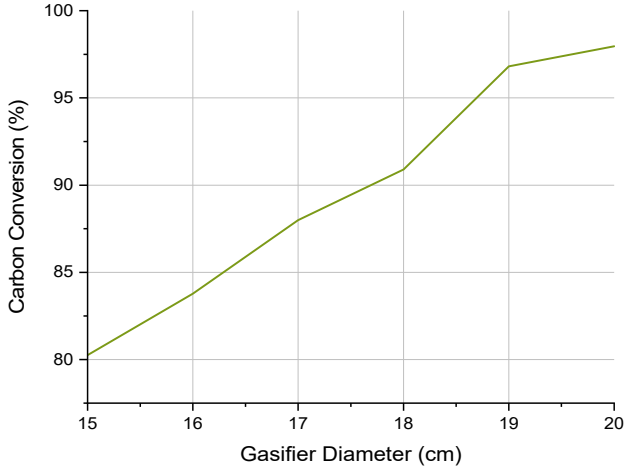

(b)

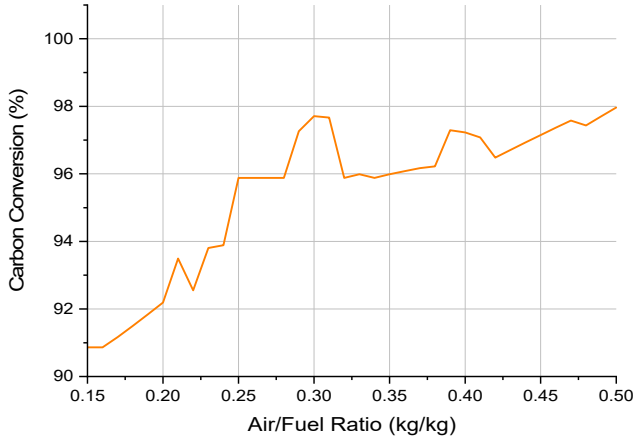

(c)

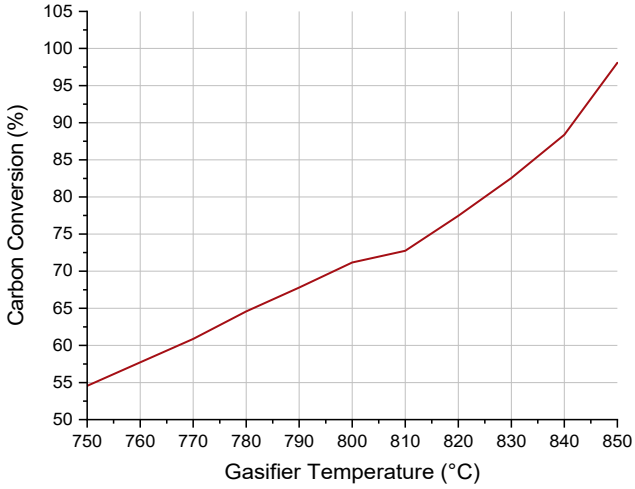

(d)

Fig. 12. Effect of operational and design parameters on carbon conversion (a) Gasifier length (b) Gasifier diameter (c) Air/fuel ratio (d) Gasifier temperature.

investigating the effect of temperature, diameter, and length on syngas composition, it is often found that the parameters are positively correlated. On the other hand, the diameter has a negative effect on the H_2 concentration. These relationships are also supported by parametric analysis results. In addition, there was no significant positive or negative correlation between the air-to-fuel ratio and any input or output parameter. This is due to the fact that different fuels and gasifier designs operate at all air-to-fuel ratios. When the effect of fuel quality on LHV and exergy is analyzed, it can be determined that although carbon has no significant relationship, hydrogen improves the calorific value of syngas while oxygen reduces it. This could be associated to decreases in combustible gas production as the oxygen content of the fuel increases. In addition, it was observed that the factors of temperature, length, and diameter improve the syngas thermal value. According to the results of a

Table 8
A brief statistical description of the dataset.

	C	H	O	Temperature	Length	Diameter
Mean	48.27	5.87	39.63	789.99	5.59	0.15
Standard Deviation	4.23	0.85	8.07	30.07	1.22	0.06
Minimum	43.90	3.46	17.82	750.00	1.30	0.03
Maximum	59.92	6.59	46.58	850.00	7.50	0.30
	H_2	**CO**	**CO_2**	**CH_4**		
Mean	0.15	0.14	0.12	0.11		
Standard Deviation	0.07	0.07	0.05	0.09		
Minimum	0.01	0.01	0.01	0.01		
Maximum	0.36	0.47	0.28	0.41		
	Air/Fuel Ratio	**LHV**	**Exergy**			
Mean	0.33	7659.14	8421.50			
Standard Deviation	0.10	2603.42	2663.72			
Minimum	0.15	2504.68	3175.17			
Maximum	0.50	16353.63	17329.49			

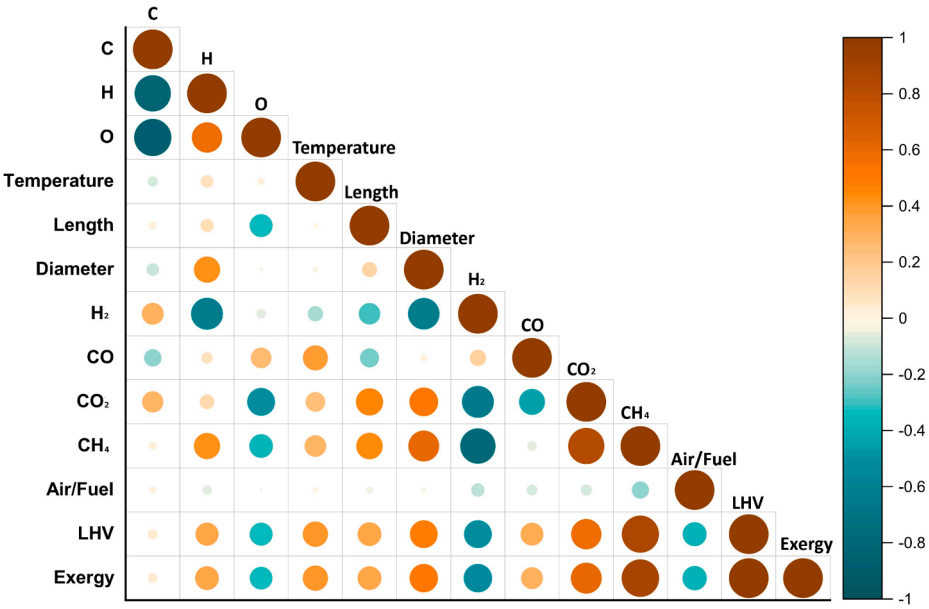

Fig. 13. The heat map for the input and output variables in the dataset created.

parametric analysis, increases in these parameters increased the concentration of combustible gases within the syngas content. Similarly, parametric testing demonstrated that increasing the air-to-fuel ratio decreased syngas' calorific value.

3.4. Design and evaluation of the ANN model

Following the data removal process, a dataset containing 258,816 input and output variables was created. The Neural Network Toolbox was used to develop, train, test, and validate the ANN model. The suggested ANN architecture includes a multi-layered perceptron structure with input, output, and hidden layers. Randomly, the dataset was split into three groups: 80% for training, 15% for testing, and 5% for validation. Fig. 14 depicts the structure of the ANN model proposed in this study.

There are 7 neurons in the input layer, 28 neurons in the first hidden layer, 12 neurons in the second hidden layer, and 6 neurons in the output layer. Carbon (db.%), oxygen (db.%), hydrogen (db.%), gasifier temperature (°C), air/fuel ratio (kg/kg), gasifier diameter (cm) and gasifier length (cm) are all input neurons. Further, H_2 (mol.), CO (mol.), CO_2 (mol.), CH_4 (mol.), LHV (kJ/kg), and exergy (kJ/kg) are the output neurons of neural network model. The ANN model's attributes are listed in Table 9.

Since there is no exact solution for calculating the number of perceptrons in hidden layers, trial and error was used. Additionally, iterations were used to fine-tune the model's parameters in order to decrease the loss function. An optimizer is a tool that determines how to modify network weights based on the output of the loss function. Fig. 15 depicts the MSE value for each set throughout the varying number of epochs.

After about 150 epochs, the MSE was resolved in 1517.1369. To avoid the network from being overfit, iterations were stopped once the optimal performance value was obtained. While the number of iterations increased, the MSE value converged to a minimal value, but after a specific number of epochs, the MSE value remained constant. This indicates that once the MSE fluctuations at a constant value, the neural network model's biases and weights remain unchanged. The R^2 highlights the correlation between the anticipated and measured values. The R^2 scores for anticipated and target elements of output variables are shown in Figs. 16, 17, and 18.

Training data is presented in blue, validation data is displayed in green, and testing data is displayed in orange for all output values. Since all output variables have R^2 values >0.99, the newly reported ANN model is able to determine syngas properties. Even though there are infrequent deviations from the diagonal line, particularly in the CO, CO_2, and thermal value assessment graphs, there is a strong relationship between the estimated and actual values. The mean absolute percentage error (MAPE) and MSE values for the training, validation, and testing

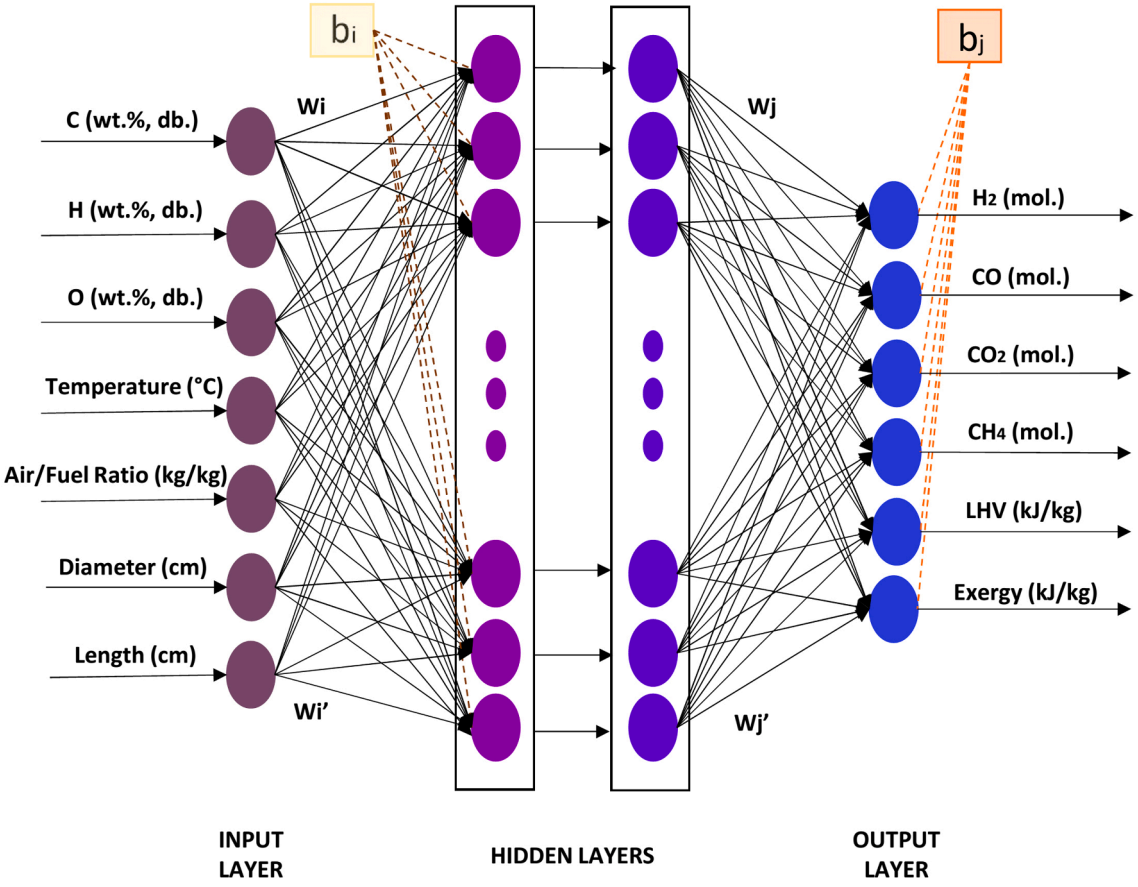

Fig. 14. The architecture of the neural network model developed in this work.

Table 9
Specifications of the ANN model.

Parameter	Value
Kind of network and algorithm for training	Feedforward backpropagation
Optimization technique	Levenberg-Marquardt
Activation function	Tangent sigmoid
Data partition by kind and portion (test, validation, and training)	Random, 15%, 5%, and 80%
Function of performance assessment	Mean squared error (MSE)
The input layer's number of perceptrons	7
The first hidden layer's number of perceptrons	28
The second hidden layer's number of perceptrons	12
The output layer's number of perceptrons	6
The maximum number of epochs	1000

data are summarized in Table 10.

The MAPE results for the training set's H_2, CO, CO_2, CH_4, LHV and exergy outputs were 1.667, 1.823, 2.121, 2.508, 0.454, and 0.380, respectively, while the MSE results were 1.08E-05, 9.63E-06, 6.65E-06, 3.68E-06, 2750.79, and 2442.47, respectively. Additionally, the MAPE results for the testing set's H_2, CO, CO_2, CH_4, LHV and exergy outputs were 1.642, 1.827, 2.139, 2.499, 0.444, and 0.372, respectively, while the MSE results were 1.03E-05, 9.96E-06, 6.65E-06, 3.73E-06, 2692.45, and 2400.86, respectively. These statistics reveal that the newly proposed ANN model can accurately predict the syngas properties for both testing and training, with a MAPE of $<3\%$.

3.5. Design and development of laboratory scale fluidized bed gasifier

As observed in the preceding sections, the ANN model was trained using diverse fuel sources, operating conditions, and design parameters. Therefore, training was undertaken using the outputs provided by the kinetic parameters for each gasifier system. In addition, data within a certain deviation range from the base case were included in the training data set for the ANN model. However, due to inaccuracies in the process simulator's calculations, not all values within the required range can be included in the data set. Given a restricted set of operational parameters or gasifier design, the ANN training technique might thus be avoided. In this part, the fully trained ANN model was used to construct a laboratory-scale gasifier using parameters that were not included in the data set. Essentially, the process of sawdust gasification takes place in a 350 cm long and 15.3 cm wide reactor. The ANN model was tasked with developing a 150-centimeter-long, 11-centimeter-diameter (base case) reactor. Consequently, a feedstock material will be pre-designed in a lab-scale gasifier where it has never previously been used in experimental or modeling work. Fig. 19 illustrates the syngas compositions of the sawdust sample in a laboratory scale gasifier designed by ANN.

As anticipated, raising the gasifier's temperature increased the concentrations of CO and H_2. It is also important to note that CH_4 and CO_2 concentrations are increasing. These patterns are similar to those seen in the chapter on parametric analysis during the gasification of juliflora chip samples. The CO content increased from 3.12 to 12.55%, whereas the H_2 concentration increased from 24.62 to 35.41%. At elevated temperatures, the advance of water–gas, which is a fundamental heterogeneous endothermic process, may explain the increase in CO and H_2 levels. Further, The CO_2 concentration increased from 7.33 to 15.68%, and the CH_4 concentration increased from 0.01 to 3.98%. Considering these changes, it can be said that heterogeneous methanation and combustion reactions are still dominant. In contrast, the concentration variation charts of the gas components differ from those from the parametric analysis investigation. Given that the parameters of the ANN

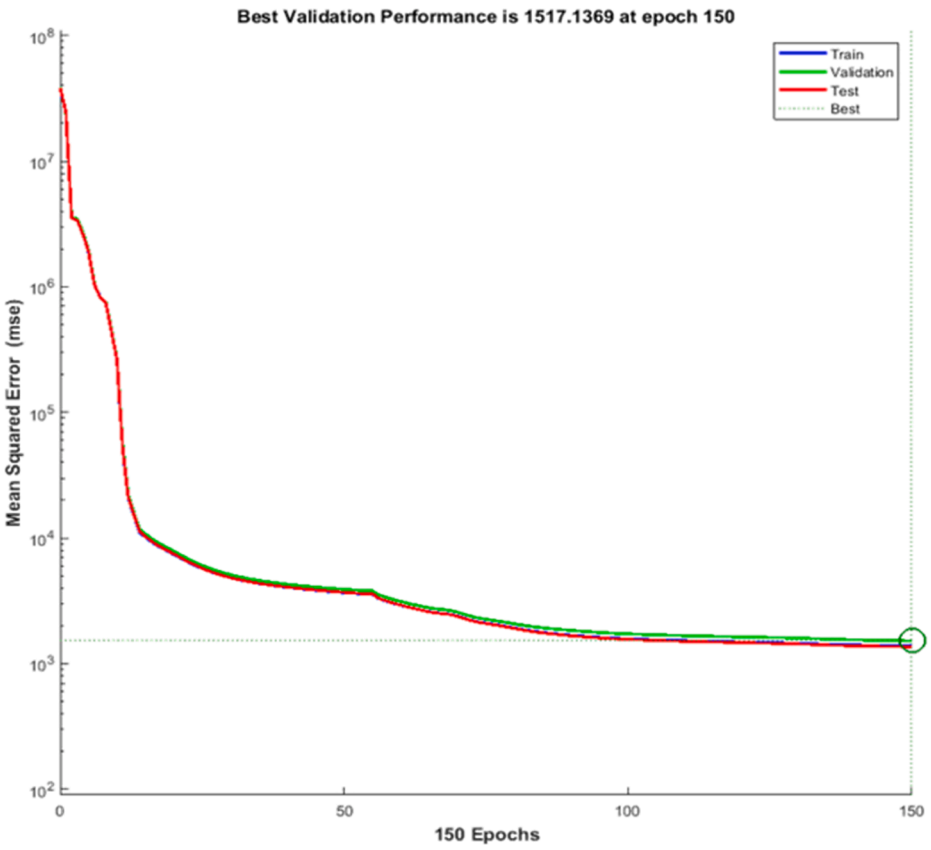

Fig. 15. In terms of MSE, performance analysis of validation, test, and training data sets.

model and the optimum kinetic parameters for the juliflora chips model are not identical, this is to be expected. The concentration change of gas components differs from the parametric analysis when the effect of gasifier length on the composition of syngas is investigated. CO concentration rises with increasing gasification length, especially above 1.75 m. The CO concentration increased from 6.83 to 13.46% between 1.00 and 2.00 m. While the H_2 concentration is steadily decreasing, the CH_4 concentration is rapidly increasing, particularly above 1.50 m. The H_2 concentration decreased from 35.36 to 21.56%, and the CH_4 concentration increased from 0.01 to 4.33%. Note that as gasifier length increases, methanization processes become dominating. In addition, the changes in gas component concentrations as a function of the gasifier's diameter were found to be in excellent accordance with the results of the parametric analysis. The CO concentration increased from 6.17 to 10.31%, and the H_2 diminished from 32.38 to 30.96%. Additionally, the CH_4 improved from 0.01 to 1.67%, and the CO_2 concentration increased from 14.93 to 15.59%. Carbon conversion increases as gasifier diameters increase, indicating that heterogeneous processes predominate. The variation in the last operational parameter, the air-to-fuel ratio, was not seen in the same manner as the results of the parametric study. As the air-to-fuel ratio increased, only the CH_4 concentration decreased, while the CO, CO_2, and H_2 concentrations changed just slightly. Typically, the concentration of flammable gases decreases as the amount of air fed to the reactor rises. However, since the elemental composition of the sawdust sample differed from that of juliflora chips and the lower reactor sizes resulted in a low carbon conversion, the amount of air supplied may not have been excessive. Hence, the endothermic reactions may have been dominated by the new operating circumstances and design parameters determined by the ANN for the sawdust sample, while the air/fuel ratio ranged from 0.15 to 0.35. These various changes observed in syngas composition naturally cause changes in syngas calorific values. Fig. 20 demonstrates the changes in syngas calorific value of operational and design variables.

Between 700 and 850 °C, there was an increase in syngas exergy and LHV. Syngas exergy improved from 4901 to 9423 kJ/kg, whereas syngas LHV increased from 3910 to 8223 kJ/kg. Due to the higher amounts of CO and H_2 components, the calorific value of syngas was improved. Identical behavior was also noticed in the findings of parametric analysis. Contrary to the results of the parametric study, the increase in syngas thermal value slows beyond 820 °C. In addition, expanding the gasifier's diameter increased the thermal value of syngas. Similar to the results of parametric analysis, the significant increase in CO and CH_4 concentrations strives to increase the thermal quality of the producer gas. The effect of increasing the length of the gasifier on the thermal value of syngas differs from the results of the parametric analysis. The thermal quality reduces as the gasifier length grows from 1.00 m to 1.75 m, and increases beyond 1.75 m. As the gasifier length increased from 1.00 m to 1.75 m, syngas exergy diminished from 8408 kJ/kg to 7067 kJ/kg, while syngas LHV reduced from 7175 kJ/kg to 6060 kJ/kg. Beyond 1.75 m, syngas exergy increased to 7121 kJ/kg, while syngas LHV increased to 6203 kJ/kg. Above 1.75 m, the CO_2 concentration declined substantially, but the CO and CH_4 concentrations increased significantly. This variation in syngas calorific value is a result of this change in syngas composition. There was a continuous reduction in exergy and LHV as the air-to-fuel ratio increased. Syngas LHV decreased from 6785 to 6038 kJ/kg, while syngas exergy declined from 7900 to 7108 kJ/kg. Owing to the remarkable improvement in N_2 content, syngas is diluted, resulting in a thermal quality loss.

Ultimately, the ANN model can be utilized to build a laboratory-scale circulating fluidized bed gasifier in place of time-consuming and computationally intensive kinetic modeling. This section shows how, given a sample within the training range of the ANN model, a previously unknown gasifier may be designed and analyzed using parametric analytic methods. Clearly, as the kinetic parameters changed for gasification processes utilizing the ANN model calculation method are different, the characteristics of syngas may vary. However, the ANN modeling's

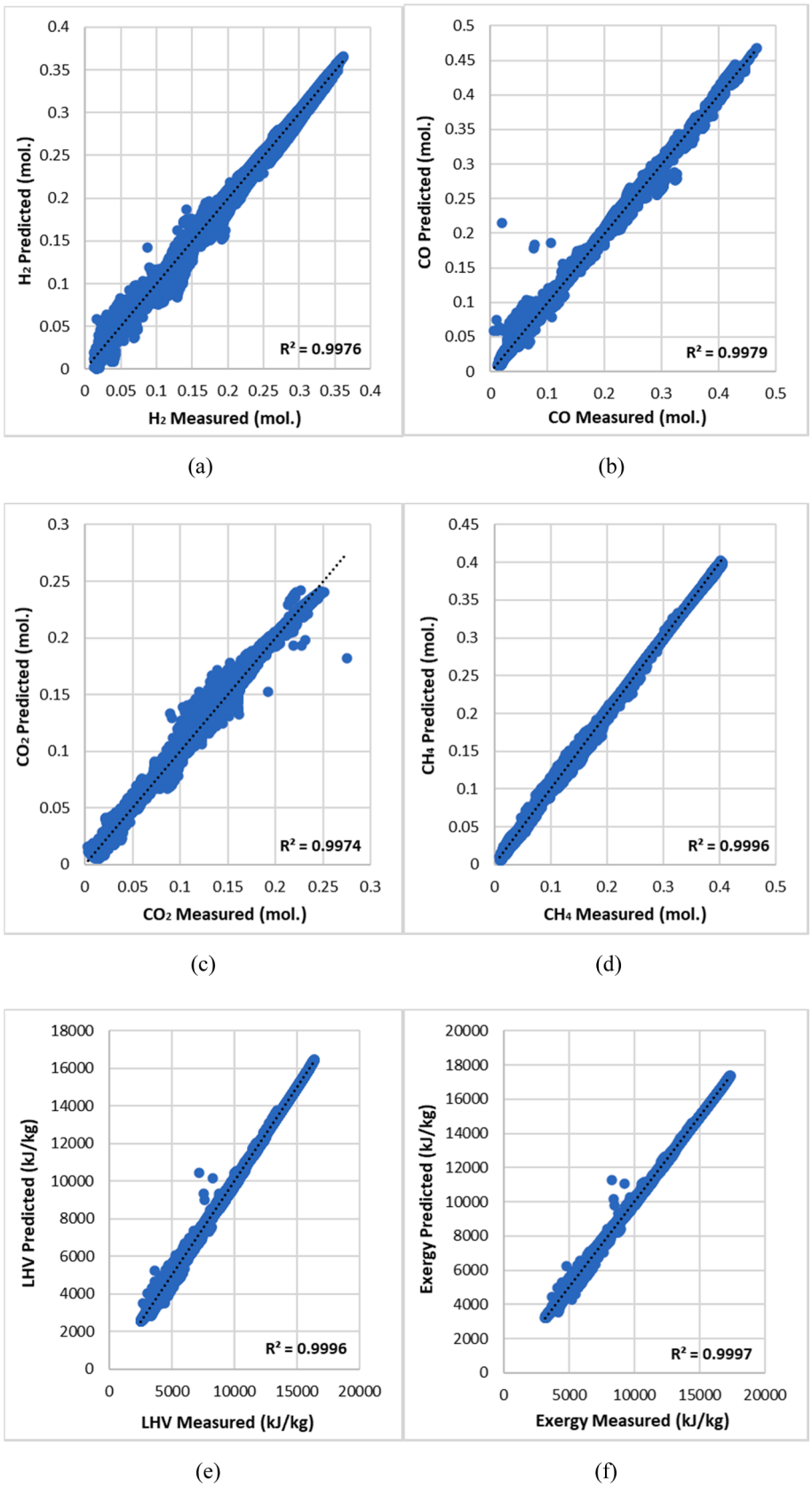

Fig. 16. R^2 results of the output variables for the training (a) H_2, (b) CO, (c) CO_2, (d) CH_4, (e) LHV, (f) Exergy.

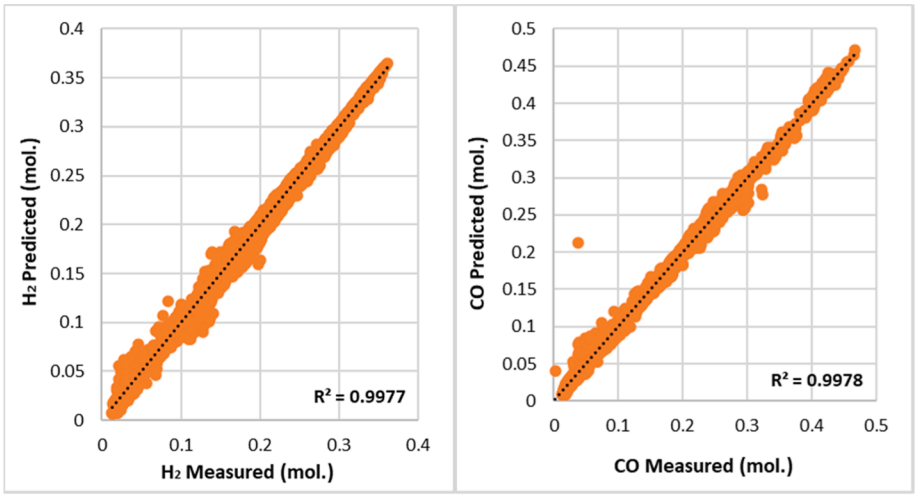

(a) (b)

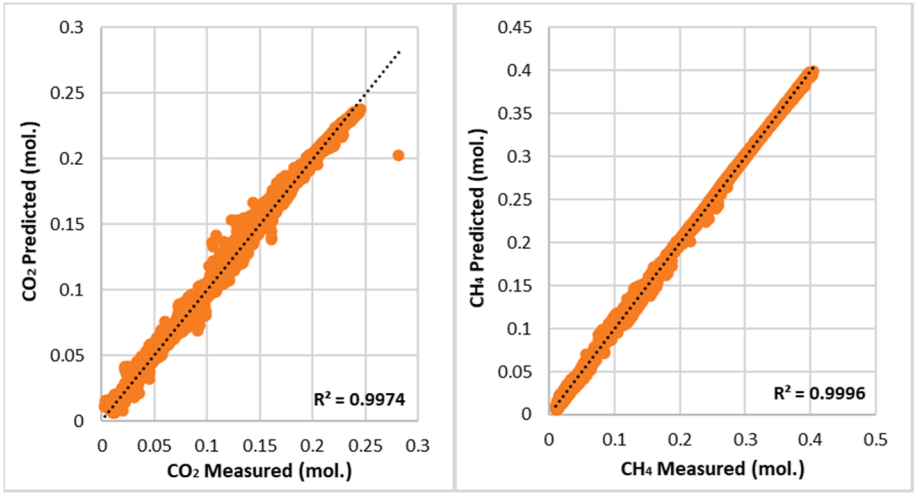

(c) (d)

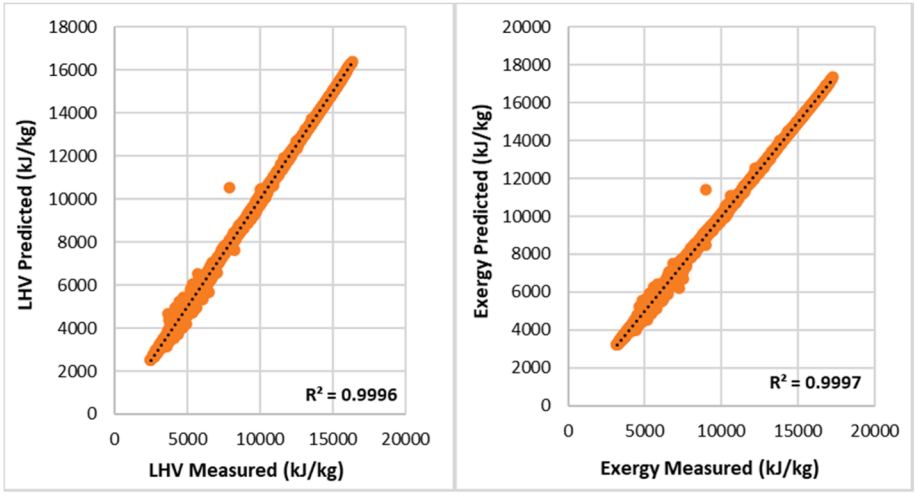

(e) (f)

Fig. 17. R^2 results of the output variables for the testing (a) H_2, (b) CO, (c) CO_2, (d) CH_4, (e) LHV, (f) Exergy.

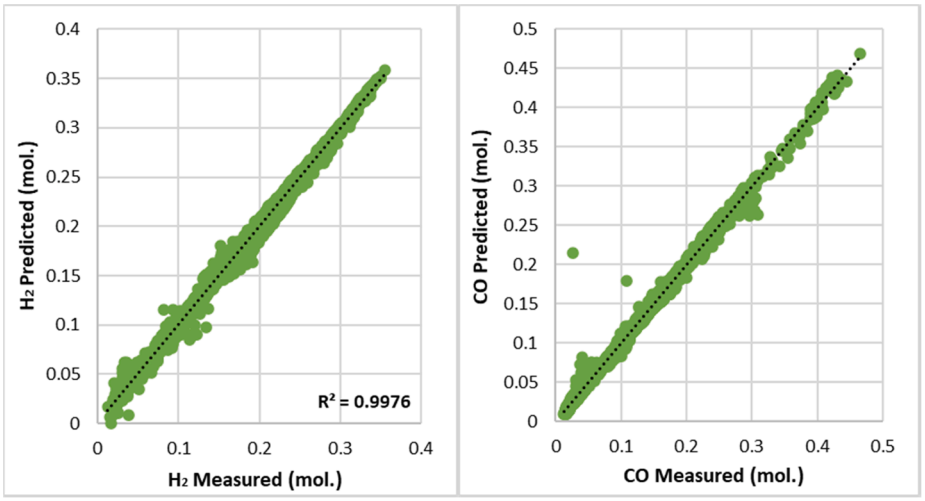

Fig. 18. R^2 results of the output variables for the validation (a) H_2, (b) CO, (c) CO_2, (d) CH_4, (e) LHV, (f) Exergy.

Table 10
MAPE and MSE results for the training, the validation, and the testing.

Dataset	Metric	H_2	CO	CO_2	CH_4	LHV	Exergy
Training	**MSE**	1.08E-05	9.63E-06	6.65E-06	3.68E-06	2750.79	2442.47
	MAPE	1.667	1.823	2.121	2.508	0.454	0.380
Testing	**MSE**	1.03E-05	9.96E-06	6.65E-06	3.73E-06	2692.45	2400.86
	MAPE	1.642	1.827	2.139	2.499	0.444	0.372
Validation	**MSE**	1.07E-05	1.23E-05	6.95E-06	3.83E-06	3040.35	2684.77
	MAPE	1.703	1.854	2.104	2.500	0.434	0.366

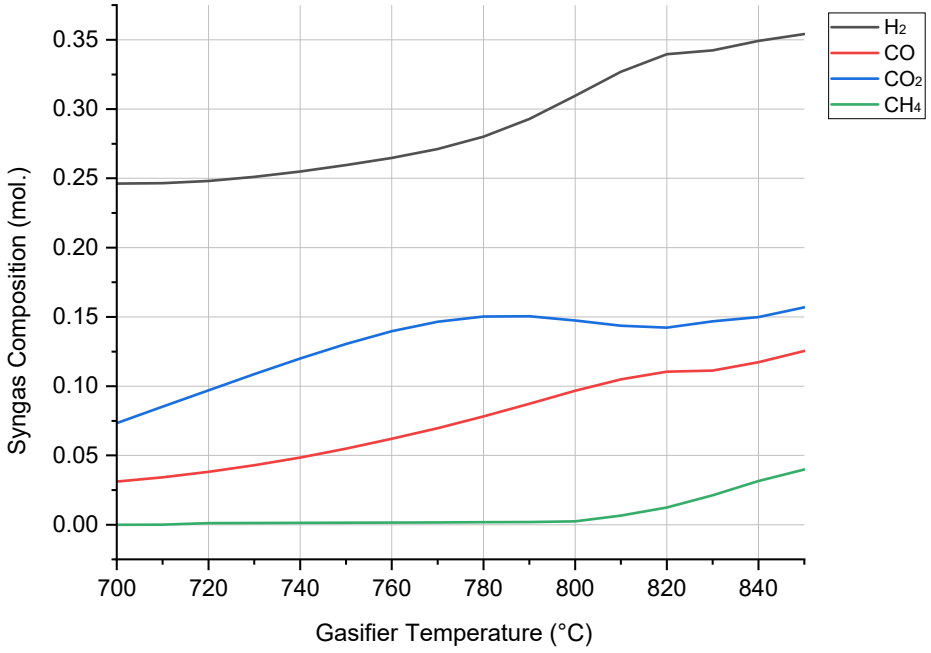

(a)

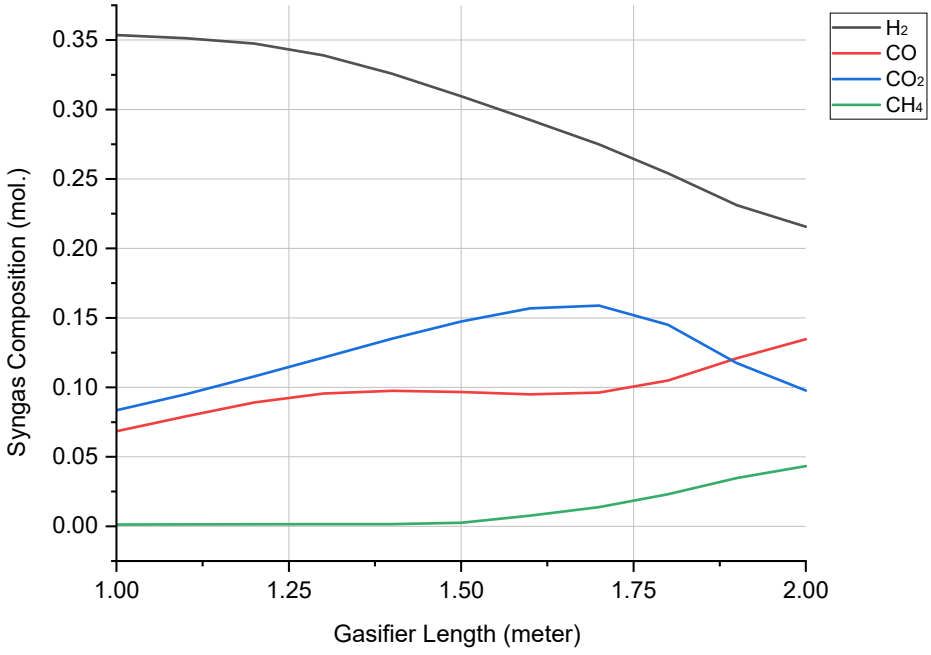

(b)

Fig. 19. Effect of design and operational parameters on syngas composition (a) Gasifier temperature, (b) Gasifier length, (c) Gasifier diameter, (d) Air/fuel ratio.

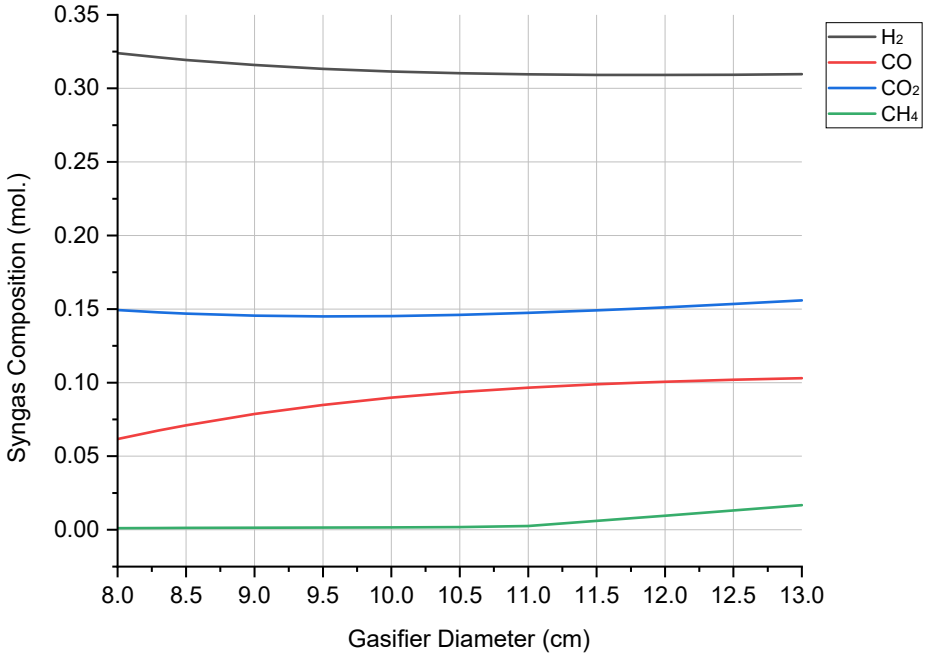

(c)

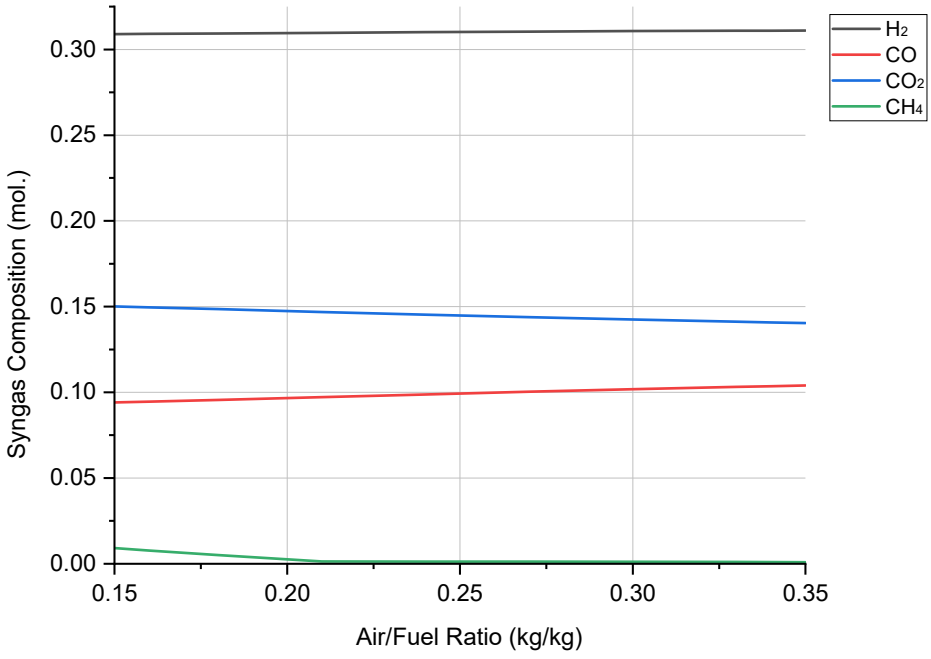

(d)

Fig. 19. (*continued*).

ability to provide a generalized gasification characteristic while simultaneously obtaining a substantial computation benefit highlights its utility.

4. Conclusion

In this paper, a 1-D kinetic model (RPlug block) for a circulating fluidized bed gasifier was proposed using the Aspen Plus process simulator. Prior to the parametric investigations, seven different gasification procedures were used to verify the circulating fluidized bed gasifier model. In parametric research, the effects of air/fuel ratio, gasifier temperature, gasifier diameter, and gasifier length on syngas characteristics were investigated. Ultimately, an ANN model was developed (including elemental composition of solid fuel, gasification conditions, and gasifier design) for a complicated gasifier system, which was trained using simulation data to predict syngas attributes and minimize computationally difficult operations. In the last chapter, a laboratory scale circulating fluidized bed gasifier was designed using the ANN model and its parametric analysis was performed. The following are the main findings drawn from this thesis research:

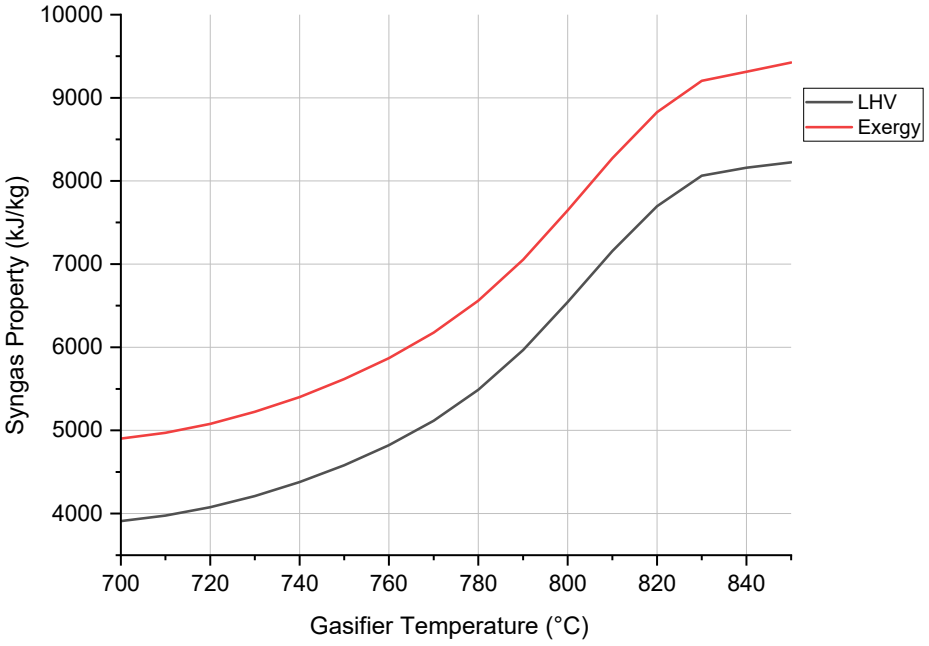

(a)

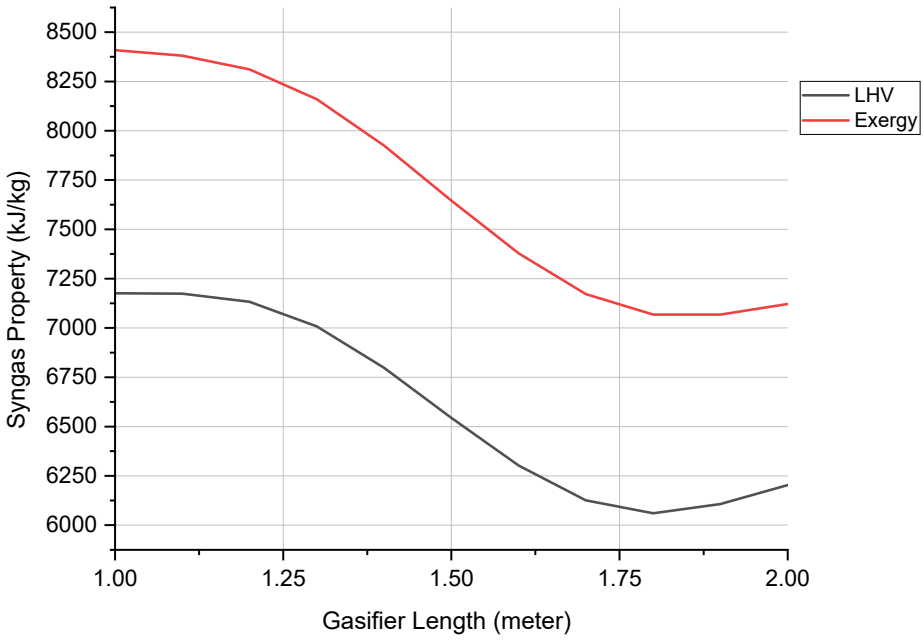

(b)

Fig. 20. Effect of design and operational parameters on syngas calorific value (a) Gasifier temperature, (b) Gasifier length, (c) Gasifier diameter, (d) Air/fuel ratio.

- Higher gasification temperatures result in higher CO and H_2 concentrations, which enhance the LHV and exergy of syngas. In addition, the diameter of the gasifier increases CO concentrations while decreasing H_2 concentrations, but the length of the gasifier increases both H_2 and CO concentrations. Both design characteristics enhance syngas' calorific value. The amount of air delivered to the reactor is also critical. The syngas composition degrades and its thermal quality diminishes as the air/fuel ratio rises.
- Heterogeneous reactions were found to be relatively prevalent in the results of the parametric analysis. The investigation of carbon conversion based on operational and design factors yielded useful results. Wide gasifier diameters and long gasifier designs have been shown to enhance carbon conversion. Additionally, the air-to-fuel ratio boosted carbon conversion, although with a fluctuating profile. It should be emphasized, however, that the gasification temperature, especially over 810 °C, is the most effective parameter in carbon conversion.
- Based on the ANN model's design for a lab-scale gasifier, it can be deduced that a gasifier length of 1.75 to 2.00 m is optimal for the sawdust gasification process. H_2 content was reduced by around 5%,

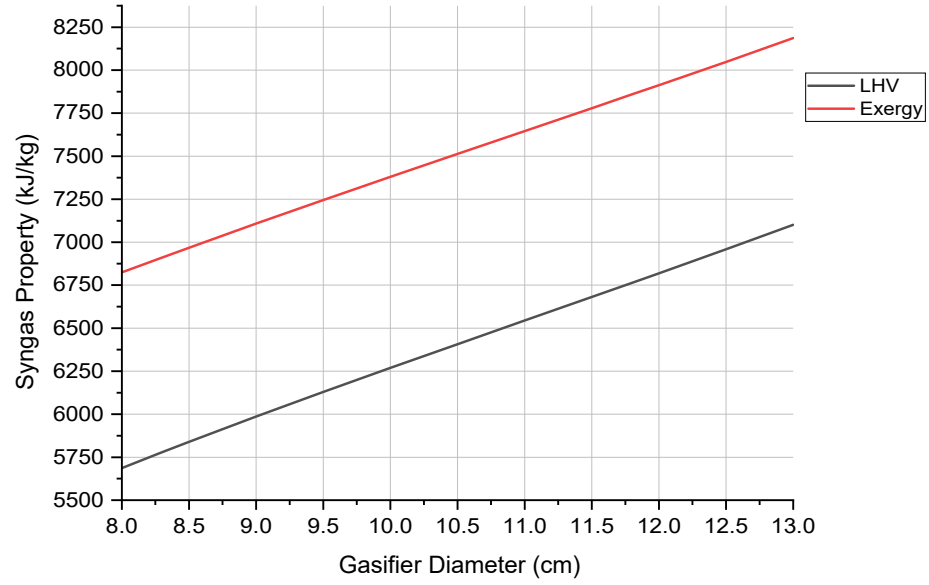

(c)

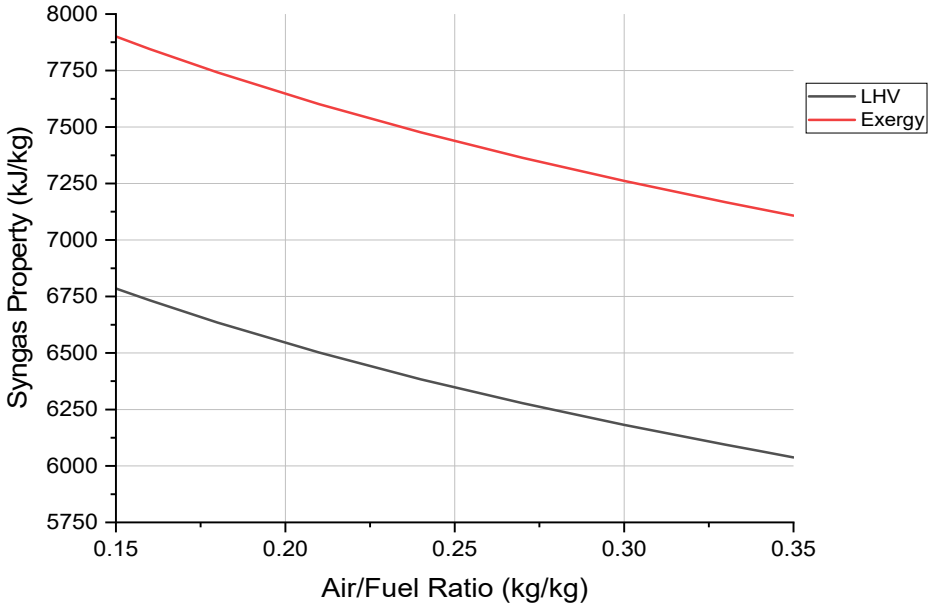

(d)

Fig. 20. (*continued*).

while CO_2 was reduced by roughly the same level. Also, beyond the heights of 1.75 m, the percentage of CO increases to 14%, and the percentage of CH_4 rises to approximately 5%.

- Between 830 °C and 850 °C, no substantial increase in syngas calorific value was detected for the lab-scale gasifier proposed by ANN. After this operating temperature, the growth in calorific value slowed. The optimal temperature for the laboratory gasifier was therefore 830 °C.
- The optimal gasifier diameter for the lab-scale gasifier developed by the ANN model is 10.5 cm. While the thermal quality of syngas constantly improves as the diameter of the gasifier increases from 8 cm to 13 cm, the composition of syngas does not follow a similar pattern. Even if CH_4 synthesis occurs at a greater diameter than 10.5 cm, the CO synthesis rate decreases and the CO_2 concentration is relatively low.
- Finding the key connections between the input and output variables required a correlation matrix. The formation of CO_2, CH_4, and H_2 was shown to be adversely affected when the carbonization degree of solid fuel decreased. The substantial positive correlation between CO_2 and CH_4 synthesis and design factors is also explained by carbon conversion. In addition, the calorific value of syngas decreases as the amount of oxygen in the solid fuel increases, but the thermal value increases as the hydrogen concentration increases. CH_4 was determined to be the most important gas component in syngas, which considerably enhanced the syngas' thermal value.
- Based on fuel properties, gasifier design parameters, and gasification operating conditions, the ANN model estimates syngas specifications with excellent precision (MAPE $<$ 3% and $R^2 > 0.99$). Thus, ANN models trained on a high-quality and large dataset may be used to analyze the system performance comprising a complicated

combination of interactions and thermochemical occurrences, such as a circulating fluidized bed gasifier.

- Although various modeling/prediction studies of gasification processes have been conducted using limited experimental datasets or datasets derived from thermodynamic modeling results, this thesis study is one of the first to consider gasifier design when predicting syngas properties for non-equilibrium modeling using ANN modeling as a deep learning technique. Despite the fact that this kinetic modeling study has limitations owing to its various assumptions, it provides a framework for future studies.

CRediT authorship contribution statement

Furkan Kartal: Data curation, Methodology, Software, Validation, Visualization. **Uğur Özveren:** Conceptualization, Data curation, Formal analysis, Investigation, Methodology, Project administration, Resources, Software, Supervision, Validation, Visualization.

Declaration of Competing Interest

The authors declare that they have no known competing financial interests or personal relationships that could have appeared to influence the work reported in this paper.

Data availability

Data will be made available on request.

Acknowledgement

This work has been supported by Marmara University Scientific Research Projects Coordination Unit under grant number FYL-2020-10139.

References

[1] Situmorang YA, Zhao Z, Yoshida A, Abudula A, Guan G. Small-scale biomass gasification systems for power generation (< 200 kW class): a review. Renew Sustain Energy Rev 2020;117:109486.
[2] Boehm RF, Yang H, Yan J. Introduction: renewable energy. Handbook of Clean Energy Syst. 2015:1–7.
[3] Sansaniwal S, Pal K, Rosen M, Tyagi S. Recent advances in the development of biomass gasification technology: a comprehensive review. Renew Sustain Energy Rev 2017;72:363–84.
[4] Giannini V, Oehmke C, Silvestri N, Wichtmann W, Dragoni F, Bonari E. Combustibility of biomass from perennial crops cultivated on a rewetted Mediterranean peatland. Ecol Eng 2016;97:157–69.
[5] Zhang Y, Zhao Y, Gao X, Li B, Huang J. Energy and exergy analyses of syngas produced from rice husk gasification in an entrained flow reactor. J Clean Prod 2015;95:273–80.
[6] Narvaez I, Orio A, Aznar MP, Corella J. Biomass gasification with air in an atmospheric bubbling fluidized bed. Effect of six operational variables on the quality of the produced raw gas. Ind Eng Chem Res 1996;35:2110–20.
[7] Ramos A, Monteiro E, Silva V, Rouboa A. Co-gasification and recent developments on waste-to-energy conversion: a review. Renew Sustain Energy Rev 2018;81:380–98.
[8] Pérez JF, Melgar A, Benjumea PN. Effect of operating and design parameters on the gasification/combustion process of waste biomass in fixed bed downdraft reactors: An experimental study. Fuel 2012;96:487–96.
[9] Jayah T, Aye L, Fuller RJ, Stewart D. Computer simulation of a downdraft wood gasifier for tea drying. Biomass Bioenergy 2003;25:459–69.
[10] Patra TK, Sheth PN. Biomass gasification models for downdraft gasifier: a state-of-the-art review. Renew Sustain Energy Rev 2015;50:583–93.
[11] Feng P, Lin W, Jensen PA, Song W, Hao L, Raffelt K, et al. Entrained flow gasification of coal/bio-oil slurries. Energy 2016;111:793–802.
[12] Ruiz JA, Juárez M, Morales M, Muñoz P, Mendívil M. Biomass gasification for electricity generation: Review of current technology barriers. Renew Sustain Energy Rev 2013;18:174–83.
[13] Basu P. Combustion and gasification in fluidized beds. CRC press; 2006.
[14] Puig-Arnavat M, Hernández JA, Bruno JC, Coronas A. Artificial neural network models for biomass gasification in fluidized bed gasifiers. Biomass Bioenergy 2013;49:279–89.
[15] Speight JG. Synthetic fuels handbook: properties, process, and performance. McGraw-Hill Education; 2020.
[16] Costa M, Rocco V, Caputo C, Cirillo D, Di Blasio G, La Villetta M, et al. Model based optimization of the control strategy of a gasifier coupled with a spark ignition engine in a biomass powered cogeneration system. Appl Therm Eng 2019;160:114083.
[17] Sharma P, Sen S, Sheth PN, Mohapatra B. Multizone model of a refused derived fuel gasification: a thermodynamic Semi-empirical approach. Energy Convers Manage 2022;260:115621.
[18] Singh DK, Tirkey J. Process modelling and thermodynamic performance optimization of biomass air gasification fuelled with waste poultry litter pellet by integrating Aspen plus with RSM. Biomass Bioenergy 2022;158:106370.
[19] Tavares R, Monteiro E, Tabet F, Rouboa A. Numerical investigation of optimum operating conditions for syngas and hydrogen production from biomass gasification using Aspen Plus. Renewable Energy 2020;146:1309–14.
[20] Trninić M, Stojiljković D, Manić N, Skreiberg Ø, Wang L, Jovović A. A mathematical model of biomass downdraft gasification with an integrated pyrolysis model. Fuel 2020;265:116867.
[21] Kartal F, Özveren U. A comparative study for biomass gasification in bubbling bed gasifier using Aspen HYSYS. Bioresource Technology Reports 2021;13:100615.
[22] Babu B, Chaurasia A. Heat transfer and kinetics in the pyrolysis of shrinking biomass particle. Chem Eng Sci 2004;59:1999–2012.
[23] Pashchenko D. Flow dynamic in a packed bed filled with Ni-Al2O3 porous catalyst: experimental and numerical approach. AIChE J 2019;65:e16558.
[24] Enget C, Jaojaruek K. CFD modeling of a downdraft gasifier with woodchips used as feedstock. Int Energy J 2020;20.
[25] Lim J-H, Bae K, Shin J-H, Kim J-H, Lee D-H, Han J-H, et al. Effect of particle–particle interaction on the bed pressure drop and bubble flow by computational particle-fluid dynamics simulation of bubbling fluidized beds with shroud nozzle. Powder Technol 2016;288:315–23.
[26] Wu Y, Zhang Q, Yang W, Blasiak W. Two-dimensional computational fluid dynamics simulation of biomass gasification in a downdraft fixed-bed gasifier with highly preheated air and steam. Energy Fuels 2013;27:3274–82.
[27] Murugan P, Sekhar SJ. Species-Transport CFD model for the gasification of rice husk (Oryza Sativa) using downdraft gasifier. Comput Electron Agric 2017;139:33–40.
[28] Raza N, Ahsan M, Mehran MT, Naqvi SR, Ahmad I. Comparative hydrodynamics study of fluidized bed gasifier incorporating static and rotating air distributor plates: A CFD approach. Powder Technol 2022;117500.
[29] Nguyen CB, Farid MM, Scherer J, Guo Q, Gräbner M, Richter A. A hybrid particle model with advanced conversion parameters and dynamic drag model applied for the CFD modeling of an entrained-flow gasifier. Combust Flame 2022;240:112040.
[30] Hajinajaf N, Mehrabadi A, Tavakoli O. Practical strategies to improve harvestable biomass energy yield in microalgal culture: a review. Biomass Bioenergy 2021;145:105941.
[31] Agu CE, Pfeifer C, Eikeland M, Tokheim L-A, Moldestad BM. Detailed one-dimensional model for steam-biomass gasification in a bubbling fluidized bed. Energy Fuels 2019;33:7385–97.
[32] Xiong Q, Yeganeh MM, Yaghoubi E, Asadi A, Doranehgard MH, Hong K. Parametric investigation on biomass gasification in a fluidized bed gasifier and conceptual design of gasifier. Chem Eng Process-Process Intensification 2018;127:271–91.
[33] Nemtsov D, Zabaniotou A. Mathematical modelling and simulation approaches of agricultural residues air gasification in a bubbling fluidized bed reactor. Chem Eng J 2008;143:10–31.
[34] Hejazi B, Grace JR. Simulation of tar-free biomass syngas enhancement in a calcium looping operation using Aspen Plus built-in fluidized bed model. Int J Greenhouse Gas Control 2020;99:103096.
[35] Aghbashlo M, Peng W, Tabatabaei M, Kalogirou SA, Soltanian S, Hosseinzadeh-Bandbafha H, et al. Machine learning technology in biodiesel research: a review. Prog Energy Combust Sci 2021;85:100904.
[36] Yan B, Zhao S, Li J, Chen G, Tao J. A conceptual framework for biomass gasifier design using a semi-empirical model and heuristic algorithm. Chem Eng J 2022;427:130881.
[37] Kartal F, Özveren U. Investigation of an integrated circulating fluidized bed gasifier/steam turbine/proton exchange membrane (PEM) fuel cell system for torrefied biomass and modeling with artificial intelligence approach. Energy Convers Manage 2022;263:115718.
[38] Sezer S, Kartal F, Özveren U. Artificial intelligence approach in gasification integrated solid oxide fuel cell cycle. Fuel 2022;311:122591.
[39] Sezer S, Özveren U. Investigation of syngas exergy value and hydrogen concentration in syngas from biomass gasification in a bubbling fluidized bed gasifier by using machine learning. Int J Hydrogen Energy 2021;46:20377–96.
[40] Kartal F, Özveren U. A deep learning approach for prediction of syngas lower heating value from CFB gasifier in Aspen plus®. Energy 2020;209:118457.
[41] Dasappa S, Reddy V, Mukunda H, Shrinivasa U. Experience with Gasifiers for 3.7-kw Engines. Ambio 1985:275–9.
[42] Sutar KB, Kohli S, Ravi M. Design, development and testing of small downdraft gasifiers for domestic cookstoves. Energy 2017;124:447–60.
[43] Khan Z, Kamble P, Check GR, DiLallo T, O'Sullivan W, Turner ED, et al. Design, instrumentation, and operation of a standard downdraft, laboratory-scale gasification testbed utilising novel seed-propagated hybrid Miscanthus pellets. Appl Energy 2022;315:118864.
[44] Guangul FM, Sulaiman SA, Ramli A. Gasifier selection, design and gasification of oil palm fronds with preheated and unheated gasifying air. Bioresour Technol 2012;126:224–32.

[45] Küçük M, Demirbaş A. Biomass conversion processes. Energy Convers Manage 1997;38:151–65.
[46] Garcıa-Ibanez P, Cabanillas A, Sánchez J. Gasification of leached orujillo (olive oil waste) in a pilot plant circulating fluidised bed reactor. Preliminary Results Biomass Bioenergy 2004;27:183–94.
[47] Chen G, Andries J, Spliethoff H, Fang M, Van de Enden P. Biomass gasification integrated with pyrolysis in a circulating fluidised bed. Sol Energy 2004;76:345–9.
[48] Van der Drift A, Van Doorn J, Vermeulen J. Ten residual biomass fuels for circulating fluidized-bed gasification. Biomass Bioenergy 2001;20:45–56.
[49] Mallick D, Mahanta P, Moholkar VS. Co-gasification of biomass blends: performance evaluation in circulating fluidized bed gasifier. Energy 2020;192:116682.
[50] Nagaraja M, Sundaresan R. Gasification of juliflora chips in a circulating fluidized bed gasifier. Int J Energy Sci 2013;3:91–8.
[51] Cardoso J, Silva V, Eusébio D, Brito P, Boloy RM, Tarelho L, et al. Comparative 2D and 3D analysis on the hydrodynamics behaviour during biomass gasification in a pilot-scale fluidized bed reactor. Renewable Energy 2019;131:713–29.
[52] Li X, Grace J, Watkinson A, Lim C, Ergüdenler A. Equilibrium modeling of gasification: a free energy minimization approach and its application to a circulating fluidized bed coal gasifier. Fuel 2001;80:195–207.
[53] Teixeira G, Ponthieux A, Salvador S. Prediction of the gasification kinetics of a single wood char particle from a limited set of parameters. Fuel 2014;123:194–204.
[54] Gao X, Xu F, Bao F, Tu C, Zhang Y, Wang Y, et al. Simulation and optimization of rice husk gasification using intrinsic reaction rate based CFD model. Renewable Energy 2019;139:611–20.
[55] Mularski J, Pawlak-Kruczek H, Modlinski N. A review of recent studies of the CFD modelling of coal gasification in entrained flow gasifiers, covering devolatilization, gas-phase reactions, surface reactions, models and kinetics. Fuel 2020;271:117620.
[56] Westbrook CK, Dryer FL. Chemical kinetic modeling of hydrocarbon combustion. Prog Energy Combust Sci 1984;10:1–57.
[57] Gómez-Barea A, Leckner B. Modeling of biomass gasification in fluidized bed. Prog Energy Combust Sci 2010;36:444–509.
[58] Macak J, Malecha J. Mathematical model for the gasification of coal under pressure. Ind Eng Chem Process Des Dev 1978;17:92–8.
[59] Yoon H, Wei J, Denn MM. A model for moving-bed coal gasification reactors. AIChE J 1978;24:885–903.
[60] Schulze S, Nikrityuk P, Compart F, Richter A, Meyer B. Particle-resolved numerical study of char conversion processes in packed beds. Fuel 2017;207:655–62.
[61] Gerber S, Behrendt F, Oevermann M. An Eulerian modeling approach of wood gasification in a bubbling fluidized bed reactor using char as bed material. Fuel 2010;89:2903–17.
[62] Yan L, Cao Y, Zhou H, He B. Investigation on biomass steam gasification in a dual fluidized bed reactor with the granular kinetic theory. Bioresour Technol 2018;269:384–92.
[63] Liu X, Wang S, Du Y, Zheng M, Yang S, Wang H. CFD study of the thermochemical characteristics of mesoscale bubbles in a BFB gasifier. Adv Powder Technol 2021;32:2605–20.
[64] Ku X, Li T, Løvås T. CFD–DEM simulation of biomass gasification with steam in a fluidized bed reactor. Chem Eng Sci 2015;122:270–83.
[65] Abani N, Ghoniem AF. Large eddy simulations of coal gasification in an entrained flow gasifier. Fuel 2013;104:664–80.
[66] González WA, Pérez JF, Chapela S, Porteiro J. Numerical analysis of wood biomass packing factor in a fixed-bed gasification process. Renewable Energy 2018;121:579–89.
[67] Yang S, Wang H, Wei Y, Hu J, Chew JW. Numerical investigation of bubble dynamics during biomass gasification in a bubbling fluidized bed. ACS Sustain Chem Eng 2019;7:12288–303.
[68] Nikoo MB, Mahinpey N. Simulation of biomass gasification in fluidized bed reactor using ASPEN PLUS. Biomass Bioenergy 2008;32:1245–54.
[69] Wang Y, Kinoshita C. Kinetic model of biomass gasification. Sol Energy 1993;51:19–25.
[70] Chejne F, Hernandez J. Modelling and simulation of coal gasification process in fluidised bed. Fuel 2002;81:1687–702.
[71] Di Blasi C. Dynamic behaviour of stratified downdraft gasifiers. Chem Eng Sci 2000;55:2931–44.
[72] de Souza-Santos ML. Solid fuels combustion and gasification: modeling, simulation. CRC Press; 2010.
[73] Dryer FL, Glassman I. High-temperature oxidation of CO and CH4. In: Symposium (International) on combustion; Elsevier 1973.. p. 987–1003.
[74] Howard JB, Williams G, Fine D. Kinetics of carbon monoxide oxidation in postflame gases. Symp (Int) Combust Elsevier 1973.:975–86.
[75] Hottel H, Williams G, Nerheim N, Schneider G. Kinetic studies in stirred reactors: combustion of carbon monoxide and propane. Symp (Int) Combust 1965.:111–21.
[76] Yetter R, Dryer F, Rabitz H. Complications of one-step kinetics for moist CO oxidation. Symp (Int) Combust 1988:749–60.
[77] Jensen A, Johnsson JE, Andries J, Laughlin K, Read G, Mayer M, et al. Formation and reduction of NOx in pressurized fluidized bed combustion of coal. Fuel 1995;74:1555–69.
[78] Xie J, Zhong W, Jin B, Shao Y, Huang Y. Eulerian-Lagrangian method for three-dimensional simulation of fluidized bed coal gasification. Adv Powder Technol 2013;24:382–92.
[79] Jones W, Lindstedt R. Global reaction schemes for hydrocarbon combustion. Combust Flame 1988;73:233–49.
[80] Bejan A, Tsatsaronis G, Moran MJ. Thermal design and optimization. John Wiley & Sons; 1995.
[81] Kotas TJ. The exergy method of thermal plant analysis. Elsevier; 2013.
[82] P. Basu. Biomass gasification, pyrolysis and torrefaction: practical design and theory. Academic press2018.
[83] Watanasiri S, Anavi S, Wadsley MW. Modeling metallurgical processes using a chemical-engineering simulator. Fluid Phase Equilib 1993;82:55–62.
[84] Uddin MN, Li L-Z, Ahmed A, Almajhali KYM. Prediction of PVA fiber effect in Engineered Composite cement (ECC) by Artificial neural Network (ANN). Mater Today: Proc 2022.
[85] Lu F, Chen Z, Liu W, Shao H. Modeling chlorophyll-a concentrations using an artificial neural network for precisely eco-restoring lake basin. Ecol Eng 2016;95:422–9.
[86] Kayri M. Predictive abilities of bayesian regularization and Levenberg–Marquardt algorithms in artificial neural networks: a comparative empirical study on social data. Math Computat Appl 2016;21:20.
[87] Nhuchhen DR, Salam PA. Estimation of higher heating value of biomass from proximate analysis: a new approach. Fuel 2012;99:55–63.
[88] Han F, Cheng L. A Modified Levenberg-Marquardt (LM) algorithm for traffic equilibrium problem with nonadditive route costs. Procedia-Social Behav Sci 2014;138:305–13.
[89] Ozyildirim BM, Kiran M. Levenberg–Marquardt multi-classification using hinge loss function. Neural Networks 2021;143:564–71.
[90] H.P. Gavin. The Levenberg-Marquardt algorithm for nonlinear least squares curve-fitting problems. Department of Civil and Environmental Engineering, Duke University. 19 (2019).
[91] Arena U. Fluidized bed gasification. Fluidized bed technologies for near-zero emission combustion and gasification. Elsevier 2013:765–812.
[92] Kombe EY, Lang'at N, Njogu P, Malessa R, Weber C-T, Njoka F, et al. Process modeling and evaluation of optimal operating conditions for production of hydrogen-rich syngas from air gasification of rice husks using aspen plus and response surface methodology. Bioresour Technol 2022;127734.
[93] Ajorloo M, Ghodrat M, Scott J, Strezov V. Modelling and statistical analysis of plastic biomass mixture co-gasification. Energy 2022;256:124638.
[94] von Berg L, Anca-Couce A, Hochenauer C, Scharler R. Multi-scale modelling of fluidized bed biomass gasification using a 1D particle model coupled to CFD. Fuel 2022;324:124677.
[95] Wang C, Jin H. Development of kinetic model for supercritical water gasification and dynamic characteristics investigation on tubular reactor. Fuel 2022;328:125284.
[96] Rabea K, Michailos S, Akram M, Hughes KJ, Ingham D, Pourkashanian M. An improved kinetic modelling of woody biomass gasification in a downdraft reactor based on the pyrolysis gas evolution. Energy Convers Manage 2022;258:115495.
[97] Ramzan N, Ashraf A, Naveed S, Malik A. Simulation of hybrid biomass gasification using Aspen plus: a comparative performance analysis for food, municipal solid and poultry waste. Biomass Bioenergy 2011;35:3962–9.
[98] Hejazi B, Grace JR, Bi X, Mahecha-Botero A. Kinetic model of steam gasification of biomass in a bubbling fluidized bed reactor. Energy Fuels 2017;31:1702–11.
[99] Radmanesh R, Chaouki J, Guy C. Biomass gasification in a bubbling fluidized bed reactor: experiments and modeling. AIChE J 2006;52:4258–72.
[100] Li X, Yan P, Ma C, Wang J. Structural design and optimization of a solar spouted bed reactor of biomass gasification. Appl Therm Eng 2021;194:117058.
[101] Miao Q, Zhu J, Barghi S, Wu C, Yin X, Zhou Z. Modeling biomass gasification in circulating fluidized beds. Renewable Energy 2013;50:655–61.